Hydrothermal Fluid Evolution at the Maisie Gold Occurrence, Menneval, New Brunswick

By
Glen Hodge

A Thesis Submitted to
Saint Mary's University, Halifax, Nova Scotia
in Partial Fulfillment of the Requirements for
the Degree of BACHELOR OF SCIENCE
IN GEOLOGY (HONOURS)

August, 2016, Halifax, Nova Scotia

Approved: Dr. Jacob Hanley
Examining committee

Approved: Dr. Erin Adlakha
SMU PT Faculty

Date: September 1st, 2016

Contents

Hydrothermal Fluid Evolution at the Maisie Gold Occurrence, Menneval, New Brunswick

By Glen Hodge

Abstract

The Maisie gold occurrence, Menneval, New Brunswick, is hosted by Middle to Late Ordovician, fine grained clastic sedimentary rocks of the Whites Brook Formation, located within the Aroostook–Percé Anticlinorium. The Maisie occurrence consists of veins containing two generations of quartz (laminated and massive), hematite, pyrite, and trace chalcopyrite and galena. Electrum has a close spatial relationship with hematitized pyrite, and is late stage infilling vugs and fractures. "Hot" cathodoluminescence imaging of vein quartz is consistent with low grade metamorphism. Stable oxygen isotope analysis of quartz by SIMS shows relatively homogeneous $\delta^{18}O_{V\text{-}SMOW}$ values between 12.3 and 18.8‰ (Fig. 15a). Estimated initial fluid $\delta^{18}O_{V\text{-}SMOW}$ composition was between 7.0 and 18.5‰, consistent with both sedimentary-derived metamorphic waters and magmatic fluid sources, and inconsistent with meteoric or formation water. Fluid inclusion microthermometry of rare, two phase (L+V at 20^{o}C) secondary inclusions gave an average temperature of homogenization of 170.3 ± 30.8°C (1σ, n = 150), and an average salinity of 2.8 ± 2.2 wt% eq. NaCl (1σ, n = 150). Inclusion petrography (an abundance of low density vapour inclusions with rare two phase parental fluids) and isochoric data suggests rapid decompression and boiling, a potential mechanism for gold deposition. Laser Raman spectroscopy shows that minor methane and nitrogen are present in the vapour phase. The common occurrence of electrum with hematite suggests an interaction with oxidized meteoric waters, but the stable isotope and fluid salinity data do not support this idea.

Maisie is considered here to represent an epizonal-orogenic Au occurrence. Rutile found within the veins shows enrichment in tin, tungsten, and rare-earth elements, and high niobium/tantalum ratios. These characteristics do not occur in rutile found within adjacent host rocks, providing a potential indicator mineral for regional exploration.

September 1st, 2016

Acknowledgements

I would like to thank my supervisor Jacob Hanley, for giving me the opportunity to study this subject, and for all the guidance on this project. I would like to thank Jim Walker, from the New Brunswick Department of Energy and Resource Development, for giving Saint Mary's the chance to work on the Maisie deposit, and providing ample background knowledge on New Brunswick geology. I would like to thank Mike Taylor, from SLAM Exploration, for giving us access to the occurrence in Menneval. I would like to thank Brandon Boucher from the University of New Brunswick, for his help in laser ablation work. I would like to thank Mitch Kerr and Kevin Neyedley, both graduate researchers at Saint Mary's University, for their input on research and writing of this thesis.

1.0 Introduction

Sedimentary-hosted orogenic and epithermal gold occurrences formed throughout Earth's history, with examples at the Homestake Gold Mine, South Dakota, USA (Rye & Rye, 1974), the Kumtor Gold Mine, in the Issyk-Kul region, Kyrgyzstan (Mao et al., 2004), the Muruntau gold deposit, Kyzyl Kum Desert, Uzbekistan (Wilde et al, 2001), the Natalka Gold Mine, Magadan Oblast, Russia (Eremin et al., 1994), the Morila Gold Mine, Sanso, Mali (McFarlane et al., 2011), Dolaucothi Gold Mines, Dyfed, Wales, United Kingdom (Annels et al, 1989), the Saint-André-de-Ristigouche gold showing, Gaspé Peninsula, Québec (Garnier et al, 2007), deposits in the Meguma terrain of Nova Scotia, Canada (Goldfarb, 2001; Ryan and Smith, 1998), the Carlin and Jerritt Canyon deposits, Nevada, USA (Groves et al, 1998), and deposits in the Bendigo-Ballarat gold belt, Victoria, Australia (Kerrich and Wyman, 1990; Ramsay et al, 1998). These are well described occurrences and their PT conditions of formation, mechanisms for gold precipitation, and associated alteration and accessory phase mineralogy are well understood. Despite how well described these deposits are, there are still key questions remaining for sedimentary-hosted gold occurrences. For example, the source of the gold for many deposits is not constrained; possibilities include the host sediments containing sedimentary or hydrothermal gold enrichment that underwent dissolution and remobilization at a later time. Additionally, the fluids that carry gold in solution are poorly characterized. The source of fluids and the mass of fluid needed to generate large deposits is unclear. For example it is unclear how gold in the deposits of Red Lake, Ontario, Canada (Chi et al., 2006), and in the Witwatersrand Basin, South Africa (Hallbauer, 1986) has been concentrated in such

large quantities, requiring vast fluid/gold source reservoirs, and/or very high dissolved concentrations of gold tonnages.

The Maisie electrum (as found by preliminary scanning electron microscopy) occurrence near Menneval (and the similar Lavoie occurrence in Saint Quentin), northwestern New Brunswick, is an early Ordovician clastic sedimentary-hosted non-refractory electrum showing within the Aroostook-Percé Anticlinorium (APA). The Lavoie electrum showing is located ~30 km to the east of Saint Quentin (as seen by the elevated gold anomaly in Figure 1). General geological information noted here on the Maisie showing comes from Jim Walker (personal communications, 2015), of the New Brunswick Department of Energy and Resource Development. The showing is subvertical and strikes parallel to local structural geology, following the fold structures in host bedrock. Quartz veining and electrum mineralization occur south-southeast of an intermediate (dacite) porphyry intrusion. The original showing consisted of three quartz boulders containing anomalous gold found in the bed of a logging road approximately 9 km west of the town of Menneval. The area shows localized gold anomalies (Fig. 1). Grab samples and exploratory core samples show mineralization with a low sulphide and low oxide content in association with electrum, the only ore mineral.

The Maisie electrum occurrence is lacking characterization and classification, notably with respect to (i) gold and fluid source, (ii) the timing of mineralization relative to deformation, regional metamorphism, and emplacement of a nearby porphyry, and (iii) mechanisms of quartz and gold precipitation. Most importantly, as the occurrence becomes better characterized, Maisie can be placed into an overall deposit classification. This study

addresses these uncertainties and proposes exploration criteria that can be followed to better aid mineral exploration in northwestern New Brunswick. With a better understanding of the Maisie occurrence, the larger hydrothermal system it belongs to could be identified and traced beyond the occurrence itself.

More specifically in this study, samples of auriferous quartz vein and associated host rocks from the Maisie occurrence are used to constrain (i) the P-T conditions for the fluids depositing the gold and responsible for quartz vein precipitation, (ii) the source of these fluids and their possible relationship to local magmatic and sedimentary host rocks, (iii) the timing of the quartz veining, and (iv) the timing of gold deposition relative to other geological events. To characterize vein and host rock mineralogy, petrographic analysis of mineral assemblages was done using reflected and transmitted light microscopy, and scanning electron microscopy with energy-dispersive X-ray spectrometry (SEM-EDS). The trace element composition of rutile and quartz was determined by laser ablation inductively-coupled plasma mass spectrometry (LA-ICP-MS). To examine quartz composition, textures, and to delineate potential fluid sources, secondary ion mass spectrometry (SIMS) of stable oxygen isotopes and “hot” cathodoluminescence were used. Finally, to characterize fluid inclusions, laser Raman microscopy and fluid inclusion microthermometry were done.

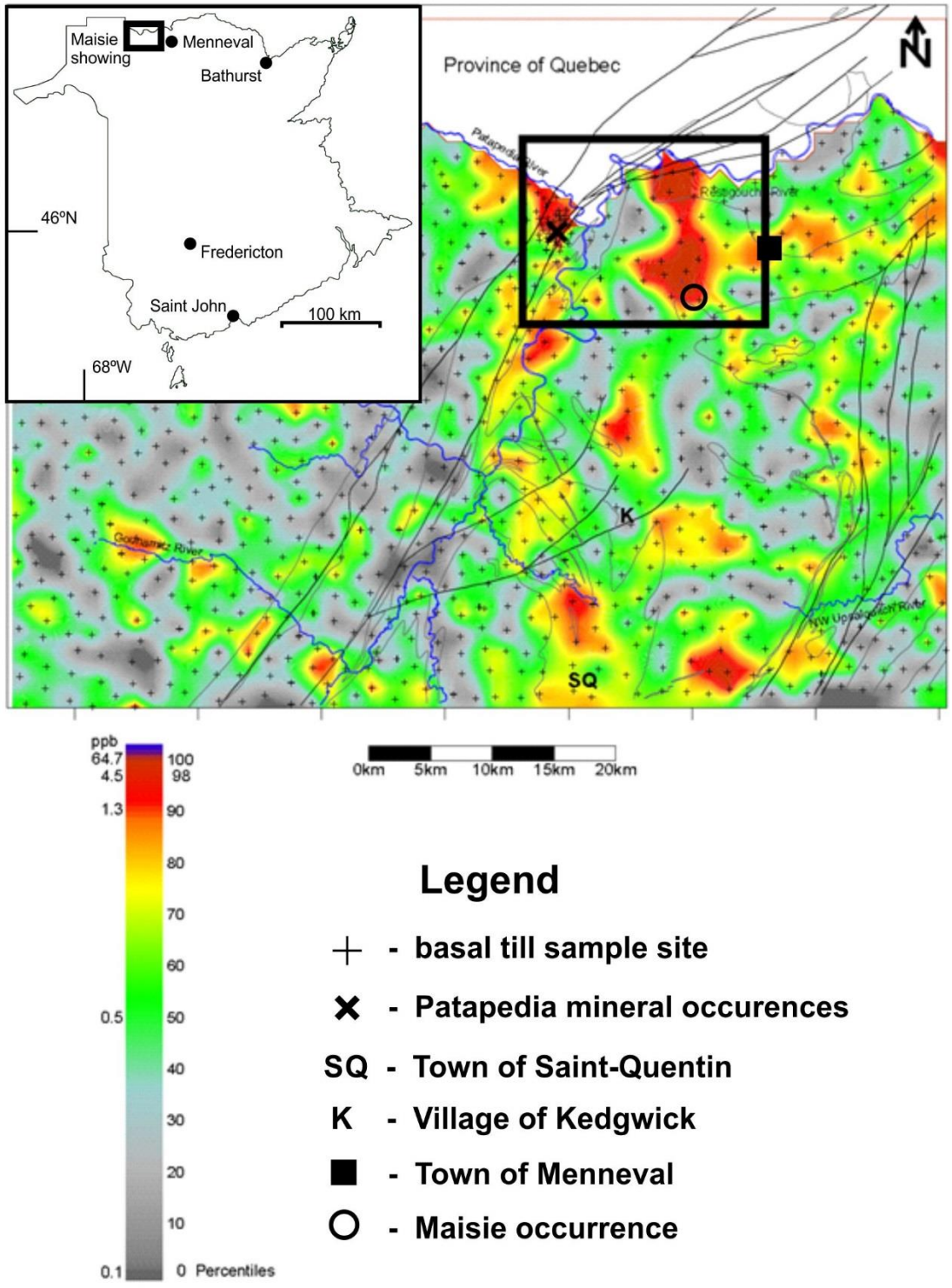

Figure 1 – Geochemical gold (ICP-MS) anomalies for northern New Brunswick. Maisie occurrence is the boxed area, showing gold values of 1.3 ppb and greater. The map has been modified from Parkhill, 2005

1.1 – Gold-mineralized systems in New Brunswick

New Brunswick hosts a variety of different gold-mineralized systems, including orogenic (Ruitenberg et al., 1989; Stirling, 1987; Watters, 1993), volcanogenic massive sulphide (VMS) (Goodfellow et al., 2003; Martin, 2006; McClenaghan et al., 2003), skarn (Lentz et al., 2002; Morrissy, 1991), and epithermal (Corbett, 2002) systems. There are three gold showings near the study area: the Saint-André-de-Restigouche Carlin-type gold showing (Garnier et al., 2007), the copper-skarn systems of the Grand Pabos Restigouche fault system (Malo et al., 2000), and the Elmtree orogenic gold deposit (Harris, 1986; Schwarz et al., 2007). The Saint-André-de-Restigouche Carlin-type gold showing in the Gaspé Peninsula is part of the far extension of the Aroostook-Percé Anticlinorium (APA), and is characterised by calcareous host rocks, a Au-As-Sb-Hg metal association, a relation with large crustal scale fault zones, and a number of felsic dykes. Mineralizing hydrothermal fluids reached temperatures of >200°C (Garnier et al. 2007). The Grand Pabos Restigouche fault system in the Gaspé Appalachians, are base metal hosting skarn deposits with gold enrichments occurring (Malo et al., 2000). The skarn systems are multi-stage with the later low temperature stage associated with the gold mineralization. Felsic dykes in the region are spatially associated with the skarn mineralization, and this relationship suggests a genetic connection between the two. The skarn deposits are characterized by argillic alteration and high salinity fluid inclusions (Malo et al., 2000). The Elmtree orogenic gold deposit (Harris, 1986; Schwarz et al., 2007) is a structurally controlled and associated with an Ordovician, sedimentary-hosted gabbroic dyke. Gold occurs as free grains attached to pyrrhotite, pyrite, and arsenopyrite. The highest gold grades are spatially associated with sulphide-rich, quartz veins peripheral to the gabbro.

The Elmtree deposit has an estimated mineral resource of 1.12 tonnes, grading 2.4 g/t gold (Castle Resources Inc., press release, 2010).

The previously mentioned deposits, not including Maisie, have unique geochemical signatures or pathfinder elements and minerals (Cu-Ag-Zn-Pb±Au: Malo et al., 2000; Au-As-Sb-Hg: Garnier et al., 2007; pyrrhotite, pyrite, and arsenopyrite: Harris, 1986; Schwarz et al., 2007), but the Maisie deposit currently lacks study of its geochemistry and volatiles. The Maisie occurrence is regionally isolated from other deposits, being ~45 km away from the next closest gold showing, which is an epithermal deposit containing gold (Thorn, 2011).

2.0 Geological Setting

2.1 – Regional geology of the Menneval area

Much of the geology of northwestern New Brunswick described has been provided by correspondence with Dr. Jim Walker (New Brunswick Department of Energy and Resource Development). The rocks of northwestern New Brunswick and adjacent southeastern Québec are of Late Ordovician to Early Devonian age sediments ± carbonate (Fig. 2). The region is divided into three northeast-southwest striking belts, which are the Connecticut Valley–Gaspé Synclinorium, the Aroostook-Percé Anticlinorium (APA), and the Chaleurs Bay Synclinorium that, in Québec are collectively included in the Gaspé Belt (Malo and Bourque 1993). In New Brunswick the Connecticut Valley–Gaspé Synclinorium and APA are included in the Restigouche Zone, whereas the Chaleurs Bay Synclinorium is included in the Tobique-Chaleur Zone (Davies 1977).

In New Brunswick the APA is separated from adjacent tectono-stratigraphic belts by the Restigouche Fault in the west and the McKenzie Gulch Fault in the east. The Restigouche Fault is the southwestern extension of the Grand Pabos Fault (Fig. 2) that, in Québec, is thought to account for up to 85 km of dextral strike slip movement (Malo and Béland, 1989). In the Gaspé Peninsula there are several gold and base metal skarn occurrences within rocks of the APA, most of which are associated with Acadian strike-slip movement along the Grand Pabos Fault system (Malo et al. 2000). In the eastern Gaspé Peninsula the Grand Pabos Fault locally marks the boundary between the APA and the Chaleur Bay Synclinorium to the south, whereas to the west the Grand Pabos Fault crosses the APA to become the Restigouche Fault. The APA is underlain by a middle Paleozoic sedimentary succession of clastic and calcareous marine sedimentary rocks of the Grog Brook and conformably overlying Matapedia groups, which are the two groups from this study area, which shall be described below.

The metamorphic grade of the rocks hosting the Maisie electrum occurrence is not high, showing vitrinite reflectance values of between 4.1% and 4.8% for samples in the area of the Maisie occurrence, suggesting that the host rocks have been metamorphosed beyond the oil window, i.e. > 160^{o}C (see samples 30784 & 30785 in Bertrand et al., 2005), but at most to upper prehnite-pumpellyite facies.

The highest vitrinite temperature obtained for the regional metamorphism in the Grog Brook group hosting the Maisie electrum occurrence is 265°C (Bertrand et al., 2005). The conditions of electrum mineralization are not known.

The lithologic unit of interest hosting the Maisie auriferous quartz veining is the Grog Brook Group, which occurs at the base of the sequence and is divided into the Boland Brook and Whites Brook formations. The Boland Brook Formation is dominated by dark greenish-grey, thin-bedded, non-calcareous mudstone, siltstone, and fine-grained sandstone (Wilson, 2003; Carroll 2003a; Wilson et al., 2004). Medium- to coarse-grained sandstone, grit, and conglomerate characterize the lowest exposed parts of the Boland Brook Formation. The Whites Brook Formation conformably overlies the Boland Brook Formation and consists of light to medium greenish grey, medium- to thick-bedded, medium- to coarse-grained, calcareous to non-calcareous sandstone and conglomerate, with thin interbeds of dark grey non-calcareous shale and siltstone. Although thickness varies considerably, the Whites Brook Formation is thought to be as much as 4000 m in the area (Carroll 2003a and Wilson et. al. 2004). The Whites Brook Formation is lithologically similar to the Garin Formation and has yielded graptolites ranging from late Caradoc to early Ashgill (~449 Ma) (Riva and Malo, 1988). The Whites Brook Formation is conformably overlain by the Pabos Formation (Matapedia Group).

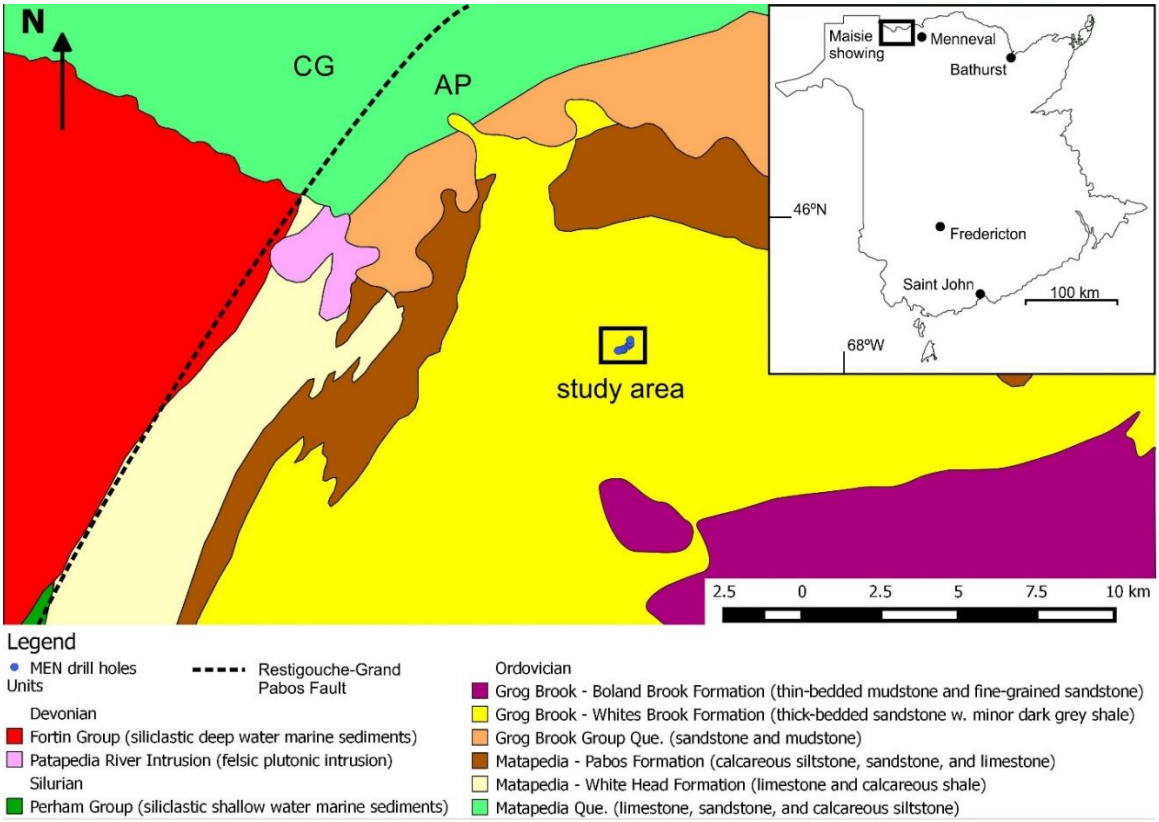

Figure 2 – Regional map of the Menneval area, New Brunswick, displaying bedrock geology that hosts the auriferous-quartz veining, as well as the two tectonic regions making up the area: CG = Connecticut Valley-Gaspé Synclinorium; AP = Aroostook-Percé Anticlinorium. The boxed 'study area' is the location within the Whites Brook formation that contains the trench and drill hole locations of Maisie.

The Matapedia Group, which conformably overlies the Grog Brook Group, is divided into the Pabos Formation and the conformably overlying White Head Formation. In New Brunswick, the Pabos Formation accounts for at least 1000 m of section and consists mainly of thin-bedded, dark greenish grey calcareous siltstone with thin sandstone laminae, interstratified with thin beds of grey carbonate-rich mudstone and minor fine-grained sandstone (Carroll, 2000, 2003a; Wilson, 2003; Wilson et al., 2004). A lower member, locally exposed at Squaw Cap on Route 17 and on the Restigouche River downstream from its confluence with the Upsalquitch River, is transitional between the underlying Whites Brook Formation and more typical Pabos lithotypes. It consists of light grey, weakly to strongly calcareous, medium-bedded, medium- to coarse-grained sandstone, siltstone and minor conglomerate, intercalated with dark grey calcareous shale (Wilson, 2003).

Finally, rare igneous intrusions occur in the Aroostook-Percé Anticlinorium. Few mafic intrusions are present, most of which occur as small lamprophyre and diabase dikes, oriented north to northeast. The largest of these, located just west of Kedgwick, can be traced for over 12km along a northwest strike, which is anomalous compared to the rest of the dikes, and it is offset by east-northeast trending faults. Another large mafic dike is located just west of the Lavoie occurrence, striking east-northeast. This dyke has returned an Ar-Ar age of 409 ± 5.9 Ma (Carroll 2003a). Two other mafic intrusions in the Kedgwick St. Quentin area, (lamprophyre and diabase), have returned ages of 376.5 ± 1.9 Ma and 391.8 ± 1.8Ma, respectively (Carroll 2003a). Felsic intrusions, composed of granodiorites, felsites, and dacites, are more abundant and tend to be spatially associated with the margins of the APA, i.e. with the major northeast striking faults such as the McKenzie Gulch and

Restigouche–Grand Pabos faults. The only dating available for felsic intrusions comes from U/Pb analysis of a biotite granodiorite dyke within a metamorphic areole produced by the Patapedia River intrusion, which gives a date of 364.4 ± 0.4Ma (Carroll 2003a).

2.2 – Bedrock geology of the Maisie occurrence

The Whites Brook Formation, which underlies both the Maisie and Lavoie occurrences, consists of up to 4000 m of light to medium greenish grey, medium- to thick-bedded, medium- to -coarse-grained, calcareous to non-calcareous sandstone and conglomerate, with thin interbeds of dark grey, non-calcareous shale and siltstone (Carroll 2003a,b).

Host rocks to electrum mineralization (Fig. 3) are all part of the Ordovician Whites Brook Formation and consist of light grey, fine-grained sandstones interbedded with dark greenish grey mudstone and siltstone. The light green mudstone is similar to that included in the Boland Brook Formation that underlies the Whites Brook Formation and crops out approximately 2.5 km to the south and south east of the Maisie showing and approximately the same distance east of the Lavoie showing. The Boland Brook Formation is characterized by millimetre scale laminations, and beds on the order of 4 to 5 cm in thickness.

A fine- to medium-grained plagioclase-biotite dacite porphyry occurs immediately west and to the north of the discovery outcrop. Trench intersections of this unit suggest that it has a northeast strike; however, at present this is not well constrained. The relationship, if any, to the quartz veins and electrum mineralization at Maisie is unknown.

2.3 – Electrum mineralization at the Maisie occurrence

27 diamond drill holes (4850 m) have been drilled, and the Maisie vein has been traced over a strike in excess of 700 m. In the west, it strikes east-northeast but becomes more northeast striking to the east of the deposit (Fig. 4). The eastern most 100 m of the vein is offset by at least three north-northwest trending, sinistral brittle faults that offset and reorient the vein to a more north-northeast strike (20^{o}-25^{o}) (Fig. 4). Additional auriferous veins have also been identified to the southeast.

Over this distance there are numerous sites where visible electrum occurs. A program of shallow drilling in 2012 and early 2013 was successful in proving the extension of mineralization to depths of 25 m (Slam Exploration Ltd., data not public at this time). To date, the highest assay was from a 4 m wide quartz vein interval grading 8.51 g/t gold that includes a 0.3 m wide interval grading 104 g/t (drill hole MG-12-26).

The bulk rock gold grades are low tangential to the porphyry in the southwest map area, and increase from <1 g/t to >10 g/t over a very short distance moving towards the northwest (Fig. 4, as marked by an arrow). The gold grades then stay high, >10g/t, for the remaining length of quartz vein. The reasons for these short distance variations in grade are not known.

a)

b)

Figure 3 – Maisie trench exposing auriferous quartz vein, northwestern New Brunswick. a) View above trench showing sediment and sedimentary rock overburden, with person for scale. b) View of walls and bottom of trenched quartz vein showing fragments of loose quartz vein material, and folded/ layered host rocks.

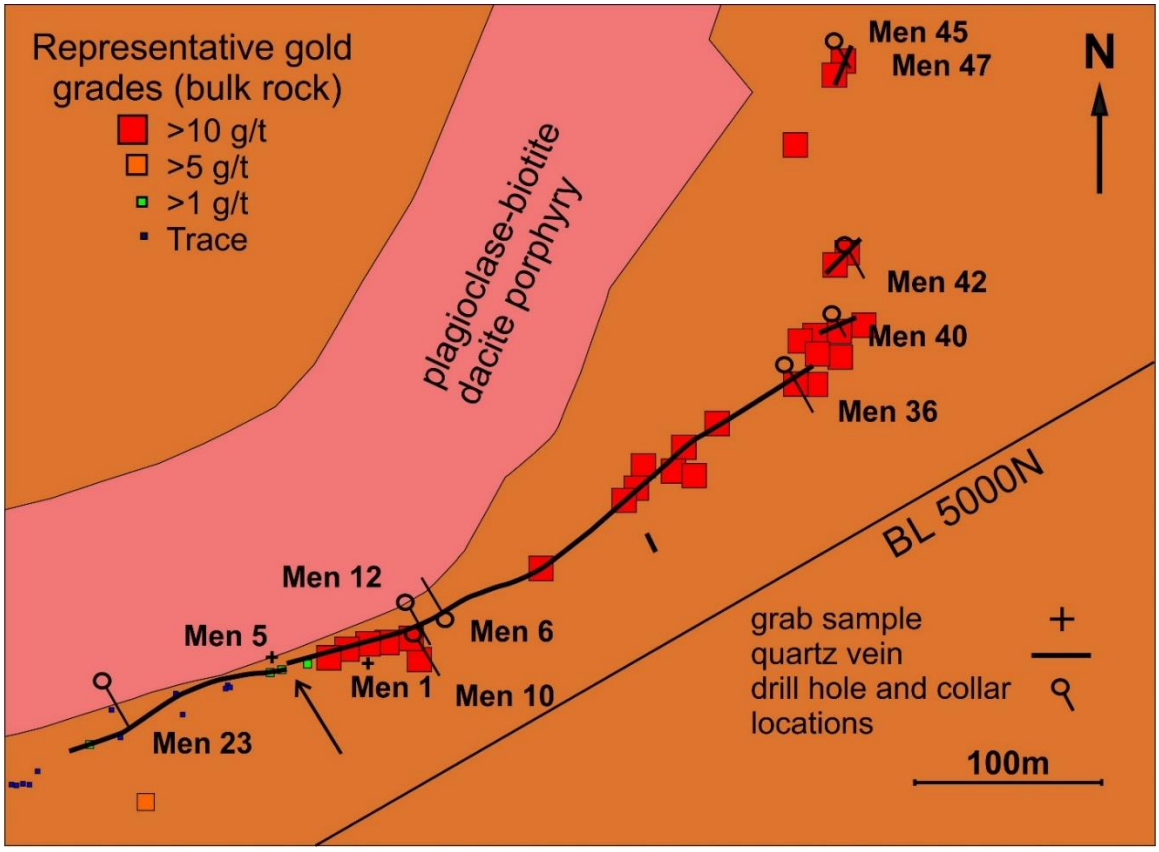

Figure 4 – Quartz vein distribution at Maisie with representative gold grades, drill hole collar locations, and projections of hole lengths to surface. BL 5000N is a SLAM grid line denoting property boundary. Note the decrease in bulk gold assays west of vein discontinuity marked with an arrow.

3.0 Methods

3.1 – Scanning electron microscopy (SEM)

SEM back-scattered electron (BSE) imaging, and energy dispersive spectroscopy (EDS) analyses of electrum and other accessory minerals were performed at Saint Mary's University using a TESCAN field emission SEM equipped with an EDS detector (Oxford Instrument X-Max 80mm^2 model). The SEM was operated at an accelerating voltage between 20 and 30 kV, beam current of 2 nA, and a working distance of 17 mm. The desktop computer software used for EDS analysis was INCA.

3.2 – Trace element analysis of quartz and rutile by LA-ICP-MS

Comprehensive trace element (LILE, HFSE, transition metals and semi metals, and REE) analysis of rutile, and the Ti content of quartz were determined by laser ablation inductively-coupled plasma mass spectrometry (LA-ICP-MS) at the Department of Earth Sciences, University of New Brunswick. The measurements were acquired using a pulsed (20 ns) 193 nm ArF Excimer laser ablation system (Resonetics RESOlution M-50) coupled to an Ar^- plasma quadrupole ICP-MS (Thermo Scientific X Series II). The ablation system employs a two-volume Laurin Technic sample cell. Measurements were done with a 10 ms dwell time for each analyte isotope, a forward torch power of 1450 W, gas flow rates of 0.8 l/min, 0.65 l/min and 6 ml/min for Ar, He and N_2, respectively, and laser fluence of 6 J/cm^2. The raw data (in cps vs. time) were quantified using the Iolite software package (Paton et al. 2011), with synthetic NIST SRM 610 glass used as an external reference material to calibrate analyte sensitivities, Ti (59.9 wt. %) as the internal standard for rutile, and Si

(~100 wt. %) as the internal standard for quartz. The BHVO-2G reference glass was used as a QC monitor.

3.3 – Fluid inclusion microthermometry

One hundred and fifty fluid inclusion microthermometric measurements in eight samples were performed on a Linkham FTIR600 heating-freezing stage mounted on an Olympus BX51 microscope at Saint Mary's University. Quartz-hosted fluid inclusions were collected from eight doubly polished thin sections, with twenty-five 1cm x 1cm wafers (Table 1) prepared. Calibration of the stage was done using synthetic fluid inclusion standards consisting of pure CO_2 (melting at -56.6°C) and pure H_2O (melting at 0˚C and homogenizing at the critical T of 374.1°C). Using these constraints, a correction for stage bias was applied to data. For temperatures above 0˚C, T_{final}=0.9865(T)+0.2959, while for temperatures below 0˚C T_{final}=0.993(T)+0.2979. Uncertainties in the microthermometric measurements were ± 0.2°C at a heating rate of 1°C/min. Salinities were calculated, from final ice melting temperatures (T_m^{ICE}), and isochores were modelled in the NaCl – H_2O system using the program SOWAT (Driesner, 2007; Driesner and Heinrich, 2007).

3.4 – "Hot cathode" cathodoluminescence

Qualitative "hot cathode" cathodoluminescence (CL) emission imaging, which provides textural information related to quartz vein formation, was done using a Lumic HC4-LM cathodoluminescence microscope coupled to an Olympus BXFM focusing mount. Images were captured by a Kappa DX40C Peltier-cooled camera operated using the DX40C-285FW software package (Lumic). The hot CL was operated at an acceleration

voltage between 12.4-13.1 kV, a beam current of 0.35 mA, a filament current of 2.3 A, a deflection of 10 V and a focus of 5.5 V.

3.5 – Stable oxygen isotopes ($\delta^{18}O$)

Stable oxygen isotope ratios of vein quartz were collected using a CAMECA IMS 7f secondary ion mass spectrometer (SIMS) at the Department of Geology, University of Manitoba. A cesium (Cs^+) primary beam with a 6.5 nA current for oxygen was accelerated (+10 kV) onto the sample surface with a sputtering diameter of 25 μm. The instrument operated with a 200 V offset, 9 kV secondary accelerating voltage, and a mass resolving power of 350. Grains of University of Wisconsin rose quartz (UWQ-1) with a $\delta^{18}O$ value of 12.3±0.1 ‰ were used for bias correction. Precision (2σ) for individual analyses was ± 1.2 ‰.

3.6 – Laser Raman microscopy/spectroscopy

Qualitative Raman spectroscopy was performed on fluid inclusions at Saint Mary's University, Halifax, to detect the presence of volatiles other than H_2O in the vapour phase at room temperature. The instrument used was a Jobin-Yvon Horiba LabRam HR confocal Raman microscope with an 800 mm spectrograph and Synapse 1024 x 256 pixel CCD detector. A 600 grooves/mm grating and 25 μm confocal hole size were used during spectrum collection. A 532 nm (green) Nd-YAG laser (105 mW laser power at source) was used for excitation. The laser beam was directed through a 100x objective. Spectrum collection (single window) over the range 1000-4200 cm^{-1} was done using an acquisition time of 40 s per accumulation and 3 accumulations per analysis.

4.0 Results

4.1 – Ore and vein petrography

All hand and core samples studied are from the Maisie trench area (Fig. 3 and 6). Quartz is the primary vein mineral at Maisie, and two generations of quartz are present: (i) larger early stage subhedral crystals (~2.5mm) and (ii) late stage veinlets of polycrystalline, subhedral-to-anhedral recrystallized quartz. Within the quartz are calcite stringers (~ 100 – 250 µm) cross cutting the quartz, and larger euhedral-to subhedral calcite growing adjacent to quartz grains (Fig. 7c and 7d). Euhedral calcite is seen in contact and intergrown with both the larger and smaller recrystallized quartz, though most in association with larger quartz. Calcite post-dates the larger generation of quartz grains, though it is in close proximity at times to the second generation of recrystallized small polycrystalline quartz (Fig. 7b). In quartz-calcite veins there are locally occurring laminations and clasts of wall rock. Wall rock clasts range 0.25 – 1 mm in size, and contain rutile grains. The laminations range 0.5 – 2 mm in width, and a few cm in length at thin section scale, though in hand sample the laminations can run 10's of cm. Quartz-calcite host accessory minerals such as pyrite, hematite, and hematitized pyrite.

Gold is present as electrum (Fig. 7e and 7f; Table 1), (Au/Ag ratio = 14.1 ± 1.9 [1σ], for n = 36 analyses over 4 samples). Electrum grains appear to be localized around hematite and/or other Fe-oxide phases and/or along micro-fractures (Fig. 5 and Fig. 9).

Table 1 – Gold (Au) and silver (Ag) analysis

Sample	Au	Ag	Au/Ag Ratio
Glen1	93.1	6.9	13.5
	93.6	6.4	14.6
	93.7	6.3	14.9
	93.3	6.7	14.0
	92.5	7.5	12.4
	92.3	7.7	12.0
	93.4	6.6	14.1
	93.8	6.2	15.2
	93.6	6.4	14.5
	92.8	7.2	13.0
	92.9	7.1	13.1
	93.2	6.8	13.7
	92.7	7.3	12.6
	92.8	7.2	12.9
Glen2	93.2	6.8	13.6
	93.4	6.6	14.2
	93.2	6.8	13.8
	93.7	6.4	14.7
	94.7	5.3	17.8
	94.4	5.6	16.8
	93.5	6.5	14.5
	94.0	6.0	15.7
	93.7	6.4	14.7
	95.6	4.4	21.9
	93.8	6.2	15.1
	92.7	7.3	12.7
	93.5	6.5	14.4
	93.7	6.3	14.8
	92.9	7.1	13.1
	91.9	8.1	11.4
	93.3	6.7	13.9
	92.9	7.1	13.2
NW4	93.4	6.6	14.1
	92.8	7.2	12.9
	93.2	6.8	13.7
Men10-2	91.0	9.0	10.1

Accessory mineral phases are pyrite, which is pseudomorphically replaced by hematite, galena, sphalerite, chalcopyrite, apatite, rutile, and monazite (Fig. 8). Additional unidentified rare earth minerals are also present. Electrum and accessory minerals appear to be late stage in relation to the quartz-carbonate veins, exhibiting open-space filling textures or fracture infilling within the veins (Fig. 7a and 7b, Fig. 8, and Fig. 9). Hematite

contents are ≤1 %, but locally may reach up to 2 % locally. Pyrite is commonly <1 %; however, oxide phases altered to pyrite may locally reach 2 %.

Rutile is found in quartz-calcite veins, included host rocks, and host rocks. Fractured, euhedral to subhedral, acicular to tabular rutile crystals, ranging from ~10 – 400 µm in length are hosted in the quartz-calcite veins (Fig. 7g & Fig. 8e/8d). Within sections of quartz-calcite veins, portions of wall rock are trapped within the vein. These pieces of included host rock contain rutile blebs (Fig. 8d). Trapped host rock rutile are smaller than rutile in veins, ranging 50 – 100 µm in size, and more tabular in shape. Wall rock contain disseminated rutile and ilmenite blebs, with the ilmenite showing varying Fe content (Fig. 7a). Ilmenite has only been observed in the host lithology. Wall rock hosted rutile blebs and ilmenite are the smallest, ranging in size from 10 – 30 µm in size.

Locally, the veins show evidence of banding (Fig. 6c). Thin bands of black material define alternating throttling events and are marked by minor amounts of sericite. The vein varies in thickness from 0.1 to 0.6 m with at least one zone up to 2.2 m wide. Several Fe phases have been listed as limonite, goethite, hematite, and pyrite (SLAM press release, 2012).

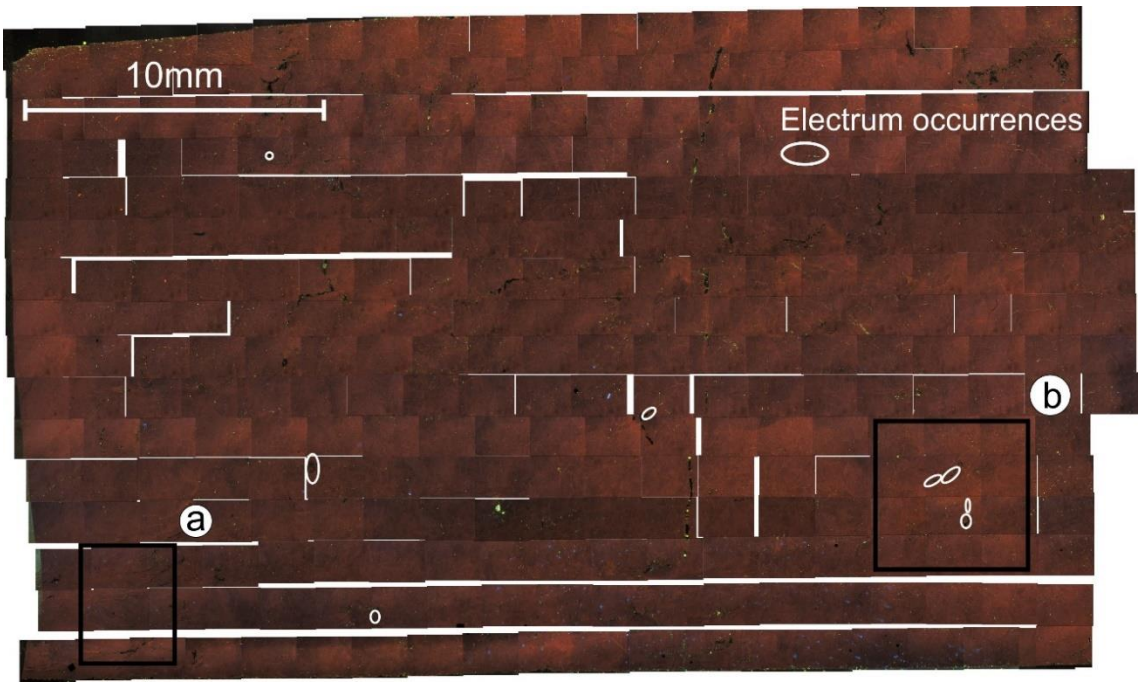

Figure 5 – CL mapped image of Maisie quartz vein sample, showing distribution of electrum mineralization. Boxed region (a) contains a previous generation laminated quartz clast, and is the region selected for SIMS analysis. Boxed region (b) is an example of electrum mineralization along fractures in the sample.

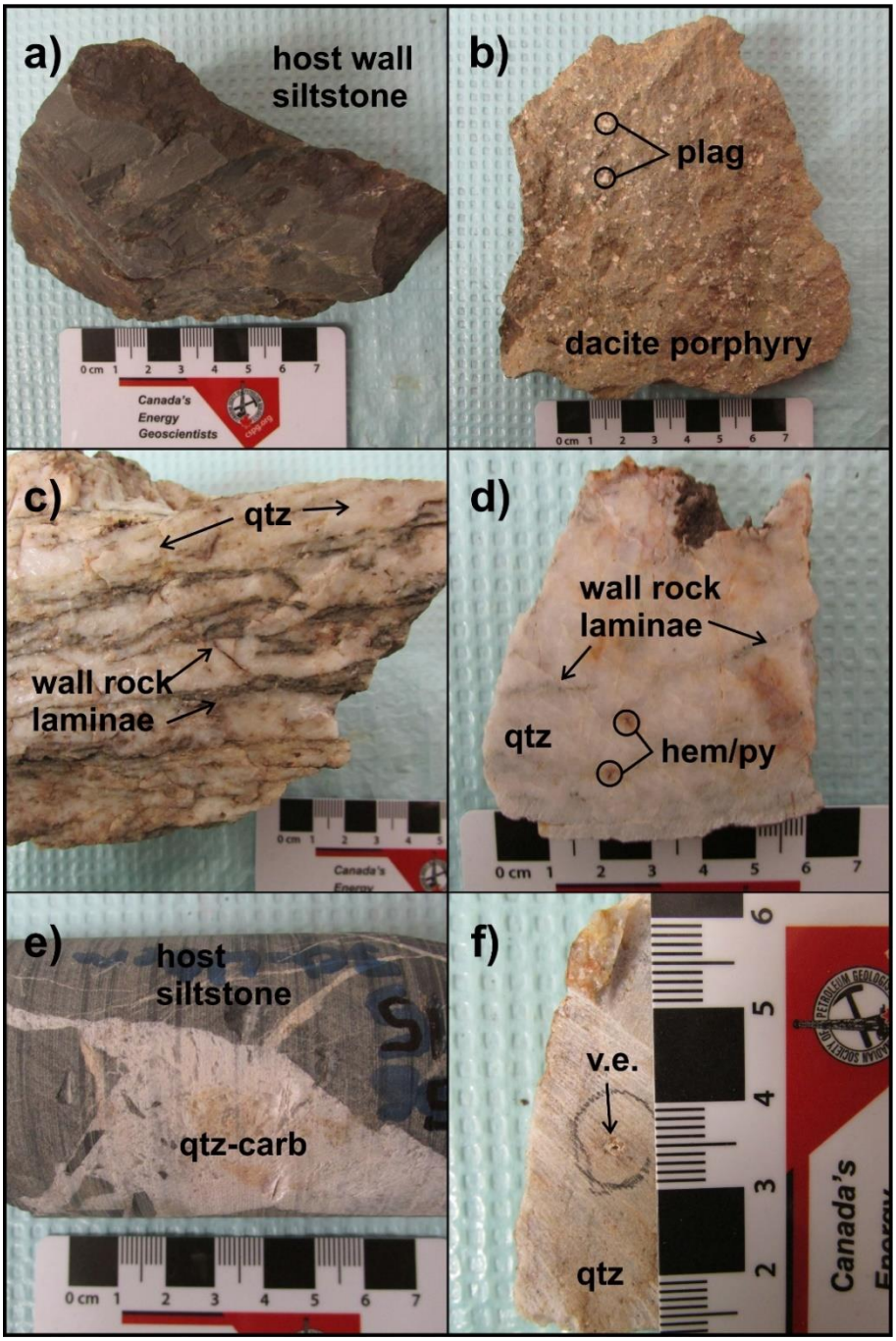

Figure 6 – Trench and core hand samples from Maisie. a) Siltstone host hand sample from trench site. b) Intermediate plagioclase (plag)-biotite dacite porphyry hand sample. c) Quartz (qtz) hand sample from trenched vein. Shows multiple lamella of wall rock trapped from crack-seal events. d) Oxidized quartz drill core sample from which fluid inclusion samples were cut. e) Siltstone host core sample with section of white quartz-carbonate (qtz-carb). f) Quartz hand sample with visible electrum (v.e.)

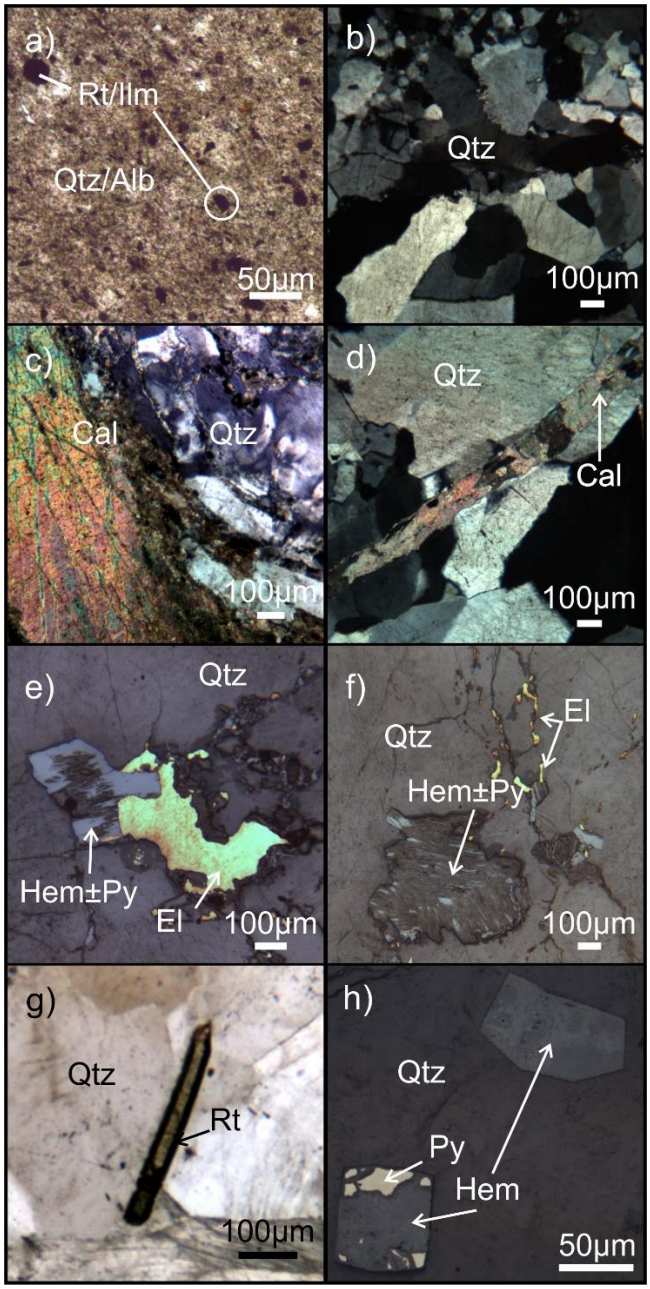

Figure 7 – Transmitted and reflected light images from host rocks and quartz veins at the Maisie occurrence. a) Siltstone wall rock hosting quartz-carbonate vein, containing disseminated rutile (rt) and ilmenite (ilm), as well as very fine grain biotite and apatite. b) Quartz (qtz) vein displaying bimodal distribution of grain size, including larger euhedral quartz grains and smaller recrystallized grains. c) Massive host calcite (cal) seen intergrown with quartz. d) Late stage calcite crosscutting quartz grains. e) Electrum (El) showing open-space filling and mutual grain boundary with hematitized (hem) pyrite (py) in quartz host. f) Electrum showing fracture infill with hematitized pyrite. g) Acicular rutile crystal in quartz vein. h) Quartz hosted hematitized pyrite crystals in various stages of retrograding.

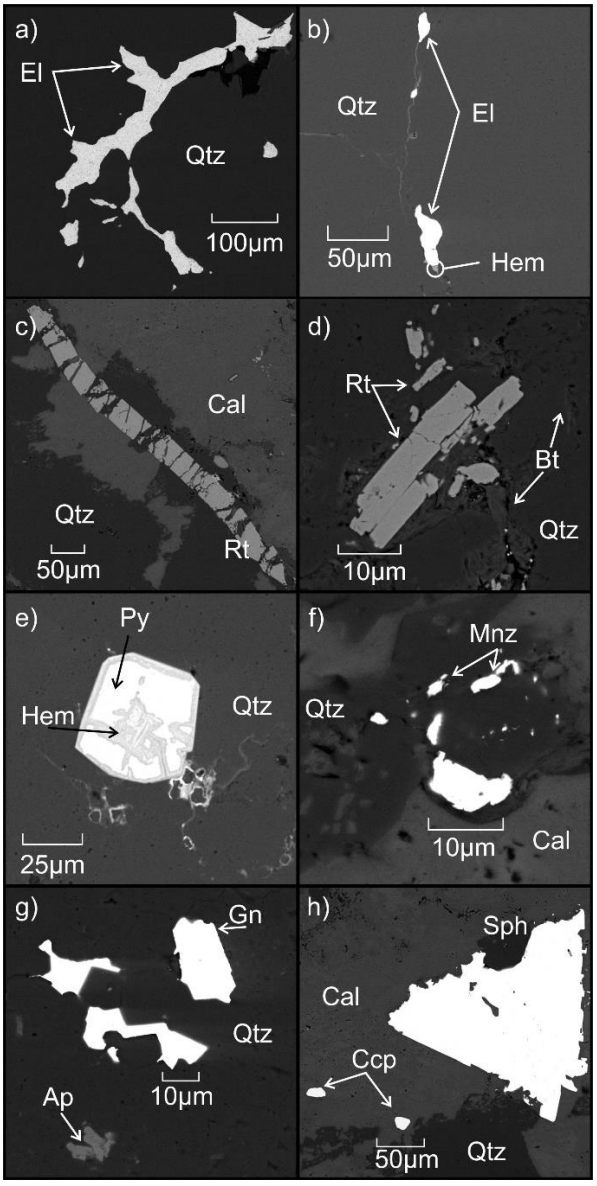

Figure 8 – BSE images of textural relationships between electrum, accessory minerals, and gange at Maisie. El = electrum; qtz = quartz; hem = hematite; cal = calcite; rt = rutile; bt = biotite; py = pyrite; mnz = monazite; ap = apatite; gn = galena; ccp = chalcopyrite; sph = sphalerite. a) Free electrum showing open-space filling textures, hosted in quartz. b) Free electrum showing fracture infill, as well as a shared grain boundary hematite, all hosted in quartz. c) Acicular rutile crystal hosted in quartz-calcite vein. d) Tabular and anhedral rutile grains hosted in quartz. e) Retrograde hematitized pyrite grain hosted in quartz. f) Anhedral monazite grains hosted in quartz-carbonate vein. g) Galena showing open-space filling textures in quartz, with euhedral to anhedral tabular apatite. h) Anhedral chalcopyrite and euhedral sphalerite hosted in quartz-carbonate vein. Sphalerite shows replacement texture by quartz-carbonate.

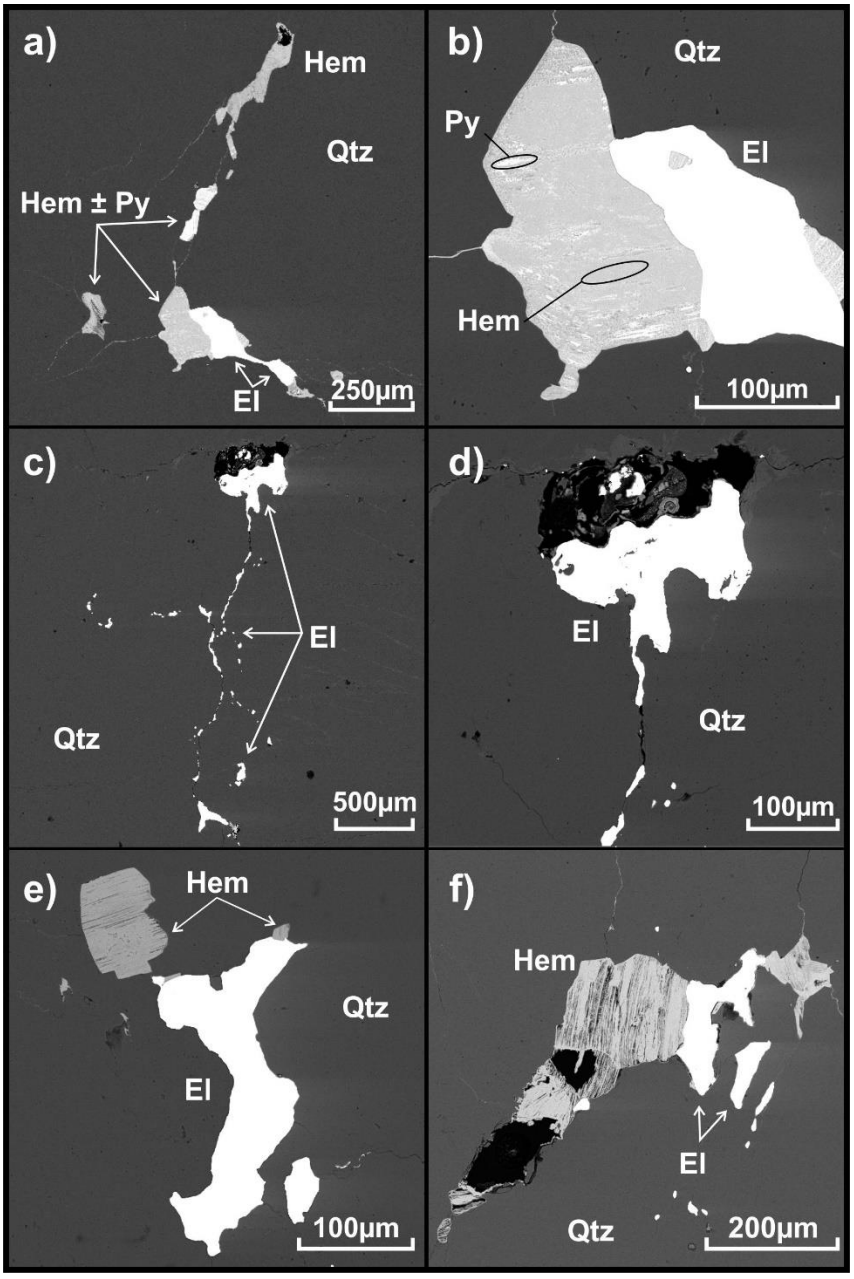

Figure 9 – BSE images and textural relationships between electrum and hematitized pyrite. a) Electrum (El), pyrite (py), and hematite (hem) showing fracture infilling within quartz (qtz), as well as a shared grain boundary between electrum and hematitized pyrite. b) Zoomed in image from (a), showing an inclusion of hematitized pyrite within electrum. c) Electrum following fracture infills and open space filling within quartz. d) Zoomed in image from (c), open space electrum. e) Electrum displaying open space filling within host quartz. Electrum also sharing a mutual grain boundary with hematite. f) Electrum and hematite showing open space filling textures and fracture infill that is related to the open space.

4.2 – Fluid inclusion petrography and microthermometry

Quartz-hosted fluid inclusions are two phase vapour-liquid inclusions, with an average inclusion size of 4 ± 1µm, and an average vapour-to-liquid ratio of 19 ± 5 (Fig. 10, type I). Along with the rare two phase inclusions analysed by microthermometry, there are empty inclusions (Fig. 10, type II) that are suspected vapour-rich or decrepitated inclusions. Inclusions are composed of aqueous H_2O and a vapour phase of air, with minor nitrogen and methane. Inclusions are indeterminate in origin, with most appearing to be secondary. Many inclusions show post trapping modification, with necking-down and abnormal crystal shape (Fig. 10b and 10d).

The measurements collected were melting point depression, freezing, homogenization, and salinity from final melting point, using 150 fluid inclusions over eight samples (Table 2). Samples Men6-2b, Men23-8b, Men36-3, Men40-2b, Men42-5b, and Men47-6c are core samples selected along the quartz vein travelling from the southwest of the map area to the northeast, with samples Men1 and Men5 being randomly selected hand samples (Fig. 4). The average salinity is 2.8 ± 2.2 eq. wt% NaCl (1σ). The average homogenization temperature is 170.3 ± 30.8°C (1σ).

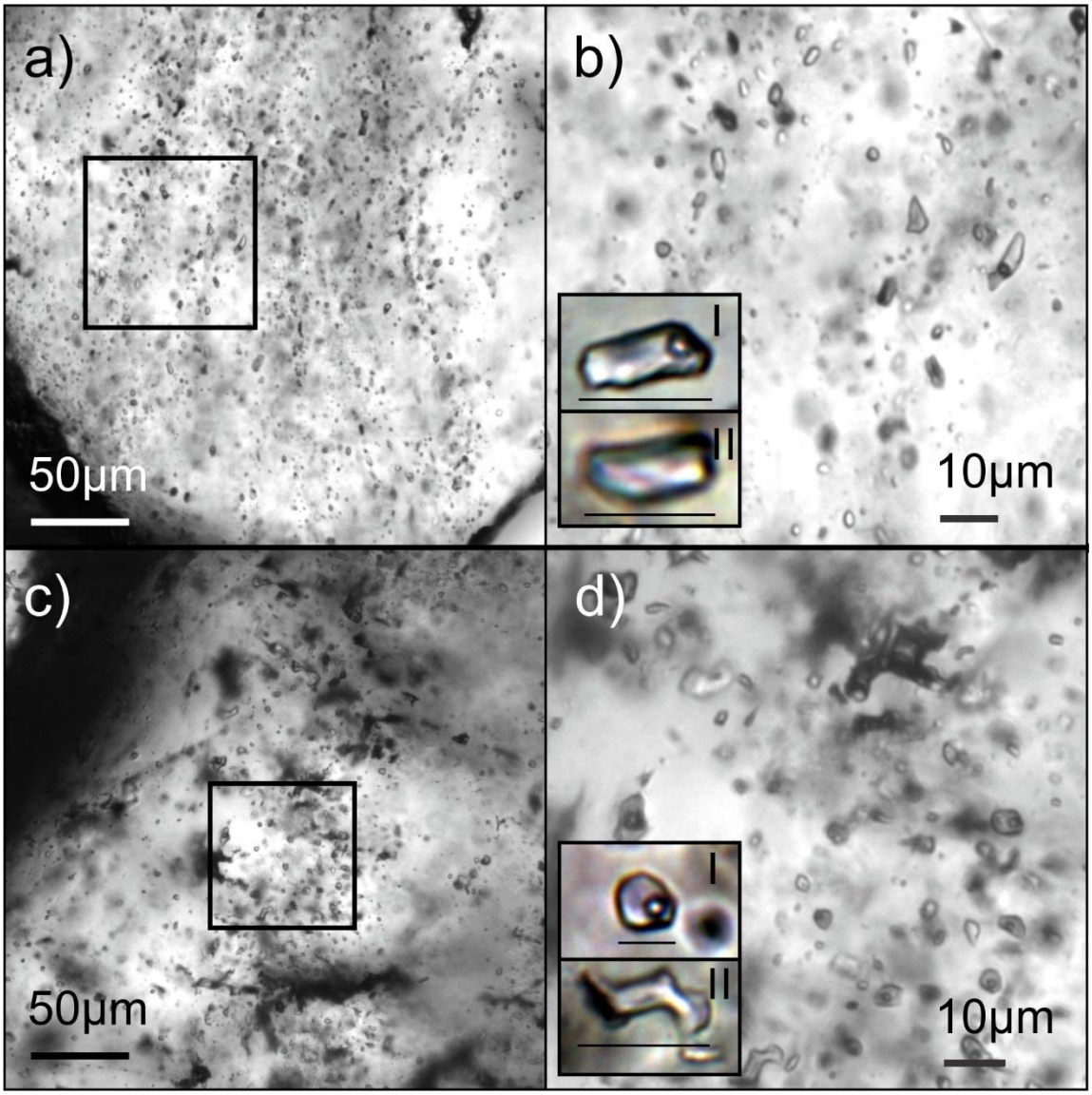

Figure 10 – Fluid inclusions from Maisie. a) Men36 fluid inclusion sample, with boxed area showing location of measured inclusions. b) Zoomed in boxed region from image 8a. I – Rare two phase liquid-vapour quartz hosted fluid inclusions. II – Empty or potential vapour rich quartz hosted inclusions. Type I and II have a line denoting 5µm. c) Men42-5b fluid inclusion sample, with boxed area showing location of measured inclusions. d) Zoomed in boxed region from image 8c. Type I shows a line depicting 4µm, and Type II shows a line depicting 6µm.

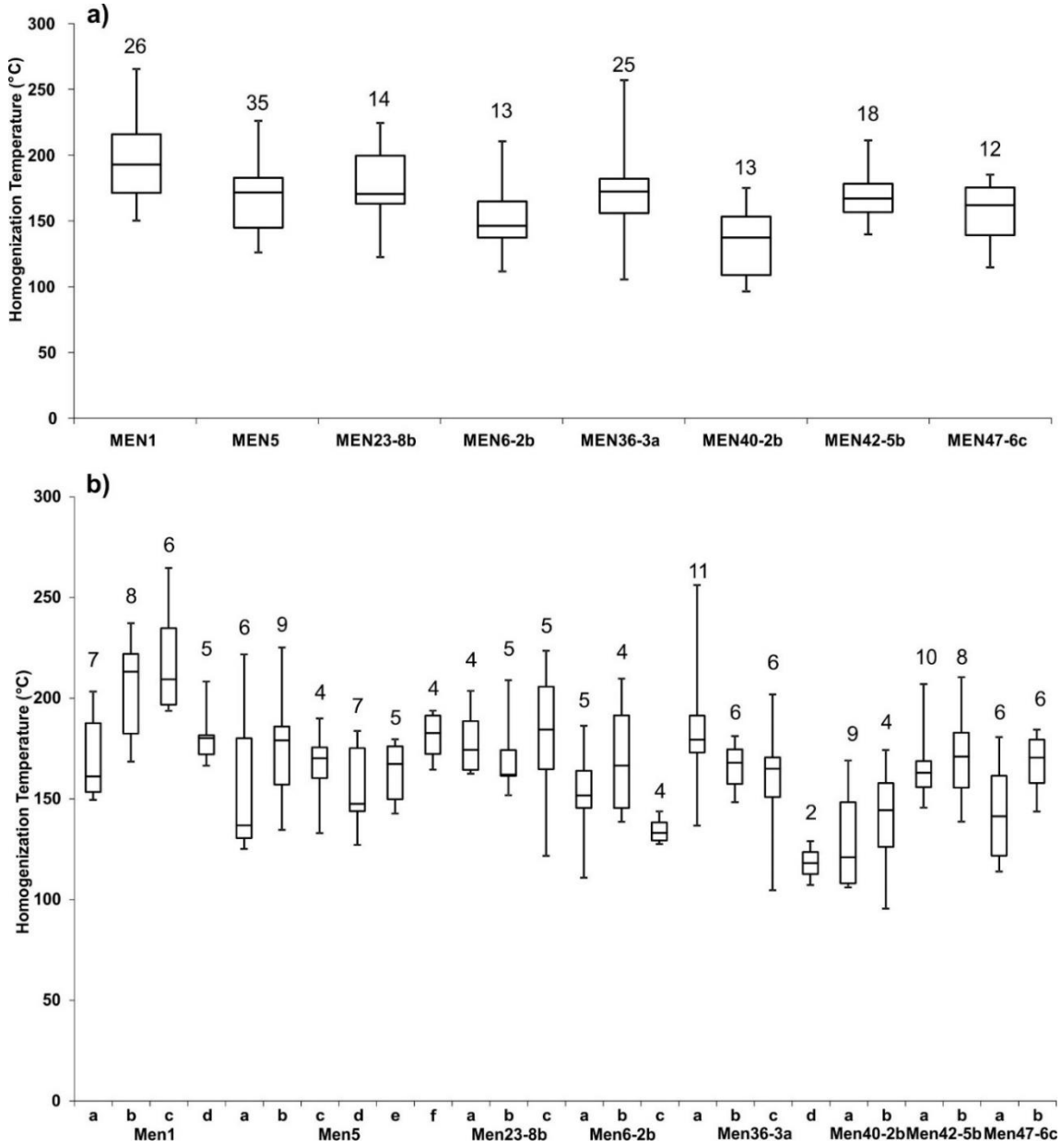

Figure 11 – Box-and-whisker plots for fluid inclusion homogenization temperatures from Maisie. The number of inclusions measured is shown by the number above each samples box. a) Variations within homogenization temperatures by whole sample. b) Variations within homogenization temperatures by sample assemblage.

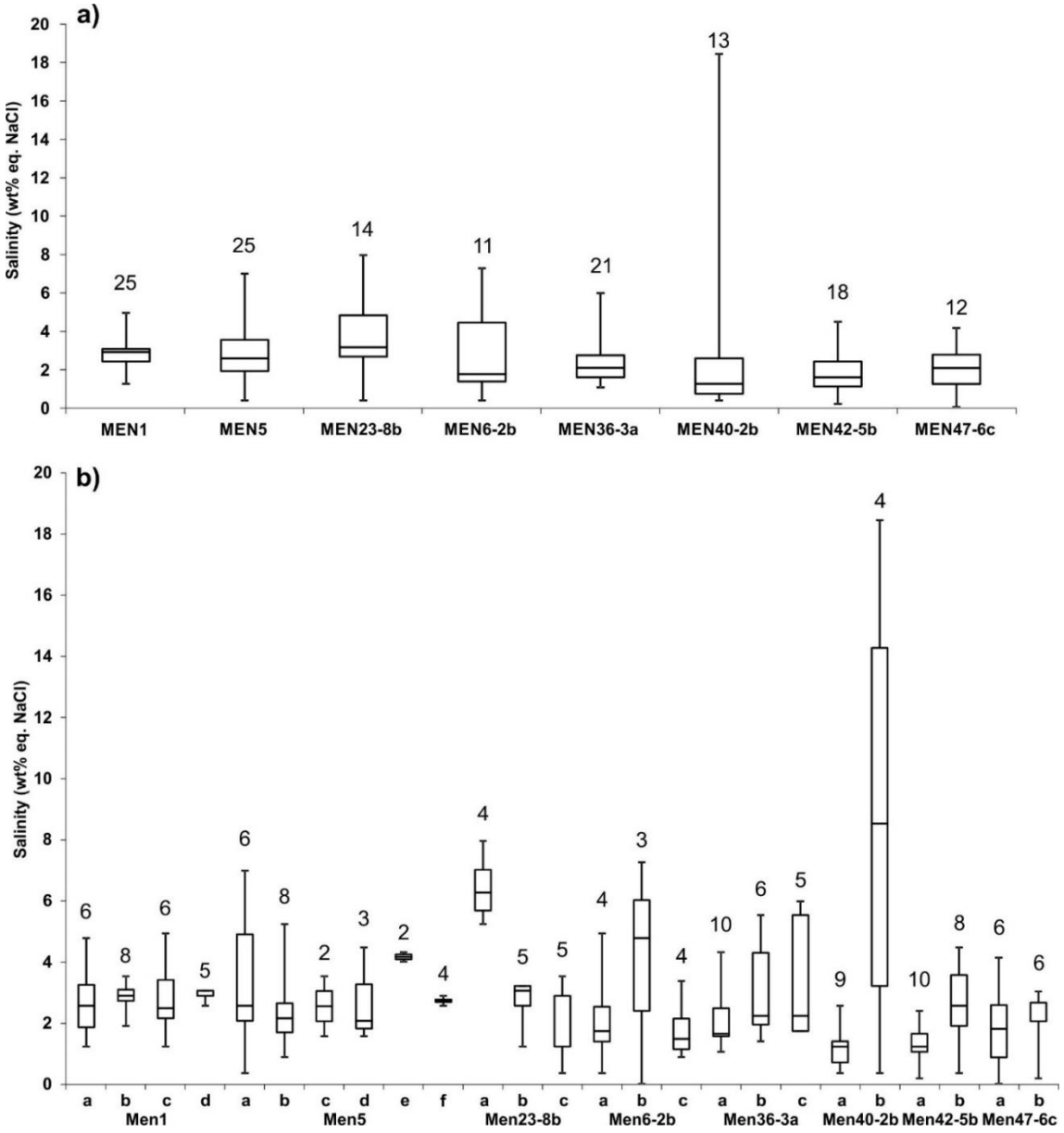

Figure 12 – Box-and-whisker plots for sample salinity from Maisie. The number of inclusions measured is shown by the number above each samples box. a) Variations within inclusion salinities by whole sample. b) Variations within inclusion salinities by sample assemblage.

Table 2 - Fluid inclusion microthermometric data.

Sample	Assem	Size (µm)	V/L[1]	T_f[2] (°C)	T_m[3] (°C)	T_h[4] (°C)	Salinity (eq. wt% NaCl)
MEN23-8b	a	3	25	-47.0	-4.2	163.1	6.70
	a	5	15	-44.6	-3.2	165.6	5.23
	a	3	15	-47.2	-5.1	184.3	7.95
	a	3	20	-46.2	-3.6	204.4	5.82
	b	3	10	-40.4	-1.8	152.3	3.04
	b	3	25	-42.3	-1.9	174.8	3.20
	b	7	15	-40.9	-1.5	162.6	2.56
	b	4	15	-43.5	-0.7	162.0	1.22
	b	2	20	-42.3	-1.9	209.7	3.20
	c	2	20	-41.8	-2.1	206.5	3.52
	c	3	25	-39.8	-0.7	165.3	1.22
	c	2	20	-42.9	-1.7	224.4	2.88
	c	5	15	-41.3	-0.2	122.0	0.35
	c	3	25	-41.9	-1.7	185.1	2.88
MEN36-3a	a	4	20	-38.9	-0.9	162.2	1.56
	a	3	20	-41.9	-2.6	234.5	4.31
	a	4	20	-40.1	-0.6	177.8	1.04
	a	4	20	-33.8	-1.3	180.0	2.23
	a	3	15	-34.4	-1.0	196.4	1.72
	a	5	15	-37.5	-1.5	187.6	2.56
	a	3	10	-38.4	-1.6	177.7	2.72
	a	5	20	-33.8	-0.8	169.7	1.39
	a	11	20	-40.6	-0.9	257.2	1.56
	a	3	15	-40.7	-0.9	184.5	1.56
	b	4	20	-40.2	-0.8	176.2	1.39
	b	5	15	-40.8	-1.1	181.9	1.89
	b	3	20	-41.1	-1.2	172.1	2.06
	b	3	25	-41.2	-1.4	164.9	2.39
	b	3	25	-45.5	-3.4	148.9	5.53
	b	3	20	-42.8	-3.0	155.7	4.93
	c	6	10	-44.6	-3.7	147.3	5.97
	c	6	15	-46.8	-3.4	202.6	5.53
	c	5	10	-40.2	-1.0	167.0	1.72
	c	5	10	-39.8	-1.3	164.1	2.23
	c	6	15	-40.4	-1.0	172.6	1.72
MEN 40-2b	a	5	10	-41.2	-0.7	169.7	1.22
	a	2	15	-41.1	-0.7	120.3	1.22
	a	3	20	-42.0	-0.6	154.0	1.04
	a	4	15	-42.1	-1.3	146.4	2.23
	a	2	15	-40.7	-0.4	121.3	0.70
	a	3	10	-40.2	-0.2	106.3	0.35
	a	3	15	-40.8	-0.8	148.9	1.39
	a	2	10	-40.1	-0.3	107.6	0.53
	a	3	10	-42.7	-1.5	108.3	2.56
	b	3	15	-57.6	-14.8	95.8	18.46
	b	3	15	-50.3	-9.0	136.8	12.89
	b	4	15	-37.6	-2.5	152.9	4.15
	b	2	25	-39.5	-0.2	174.8	0.35
MEN42-5b	a	2	20	-32.2	-0.6	146.1	1.04
	a	2	15	-40.2	-0.7	151.4	1.22
	a	2	15	-40.3	-0.6	166.1	1.04
	a	3	25	-40.0	-1.0	160.8	1.72
	a	4	15	-41.5	-1.0	170.0	1.72
	a	3	25	-41.2	-1.4	207.8	2.39
	a	2	15	-39.1	-0.7	158.1	1.22
	a	2	20	-41.5	-0.6	167.6	1.04
	a	2	15	-41.5	-0.1	178.7	0.18
	a	2	15	-42.0	-0.8	155.8	1.39
	b	8	15	-44.7	-2.1	175.9	3.52
	b	2	20	-44.5	-0.2	139.2	0.35
	b	3	30	-44.4	-2.7	146.9	4.47
	b	5	20	-43.8	-2.2	159.1	3.68

	b	3	20	-41.9	-1.6	167.4	2.72
	b	3	25	-41.5	-1.2	187.8	2.06
	b	4	15	-42.2	-1.4	182.1	2.39
	b	4	20	-42.0	-0.8	211.2	1.39
MEN 47-6c	a	5	15	-35.4	-1.3	162.3	2.21
	a	3	15	-44.0	-2.5	161.2	4.13
	a	2	20	-40.9	-1.6	181.3	2.70
	a	2	15	-40.1	0.0	122.0	0.00
	a	5	10	-40.3	-0.8	122.4	1.38
	a	3	15	-39.7	-0.4	114.3	0.70
	b	3	20	-39.6	-1.2	173.1	2.05
	b	3	15	-41.8	-1.2	169.1	2.05
	b	3	15	-42.6	-1.7	185.1	2.86
	b	3	15	-41.9	-1.2	154.9	2.05
	b	5	15	-40.8	-0.1	144.2	0.18
	b	5	15	-42.0	-1.8	182.4	3.02
MEN1	a	6	10	-41.4	-1.7	157.1	2.88
	a	5	15	-42.2	-2.0	161.8	3.37
	a	3	20	-41.0	-1.0	185.7	1.72
	a	3	20	-39.8	-0.7	204.0	1.22
	a	3	15	-43.9	-2.9	150.9	4.77
	a	4	15	-41.6	-1.3	191.0	2.23
	b	4	20	-31.3	-2.1	238.1	3.52
	b	3	25	-37.1	-1.7	235.7	2.88
	b	4	15	-37.4	-1.1	218.5	1.89
	b	4	10	-35.5	-1.7	187.3	2.88
	b	2	33	-33.2	-1.8	217.9	3.04
	b	3	20	-40.4	-1.9	209.9	3.20
	b	5	20	-41.4	-1.6	169.1	2.72
	b	2	15	-41.4	-1.6	170.5	2.72
	c	6	25	-37.4	-3.0	265.7	4.93
	c	4	20	-33.7	-0.7	195.9	1.22
	c	5	20	-41.1	-1.2	202.4	2.06
	c	3	25	-41.5	-1.4	217.8	2.39
	c	3	25	-41.7	-1.5	194.4	2.56
	c	4	33	-42.3	-2.2	241.6	3.68
	e	4	15	-31.1	-1.7	182.3	2.88
	e	3	25	-32.3	-1.8	167.1	3.04
	e	5	20	-41.5	-1.5	172.7	2.56
	e	3	25	-36.1	-1.7	180.9	2.88
	e	3	15	-41.5	-1.8	209.0	3.04
MEN5	a	5	20	-40.2	-1.5	-	2.56
	a	5	20	-29.3	-0.2	-	0.35
	a	4	20	-35.1	-	136.6	-
	a	3	20	-45.1	-4.4	129.0	6.98
	a	5	20	-39.9	-	125.6	-
	a	4	25	-41.8	-3.5	195.0	5.68
	a	4	25	-46.2	-1.5	138.0	2.56
	a	4	25	-41.2	-1.1	222.6	1.89
	b	5	15	-43.5	-1.2	135.1	2.06
	b	4	25	-44.0	-3.2	181.0	5.23
	b	4	25	-39.7	-0.5	157.6	0.87
	b	3	20	-39.8	-0.9	179.0	1.56
	b	5	20	-39.6	-	155.8	-
	b	4	15	-40.6	-1.0	179.7	1.72
	b	3	25	-40.9	-1.7	186.6	2.88
	b	4	15	-41.1	-1.3	187.6	2.23
	b	4	33	-41.9	-1.5	226.1	2.56
	c	2	20	-42.8	-2.1	171.5	3.52
	c	3	10	-39.1	-	133.4	-
	c	5	15	-39.4	-0.9	170.1	1.56
	c	4	15	-39.4	-	190.7	-
	d	2	30	-39.9	-2.7	180.2	4.47
	d	4	15	-39.3	-1.2	184.4	2.06
	d	2	25	-29.2	-	145.6	-
	d	3	20	-39.0	-	148.1	-
	d	4	10	-39.2	-	127.6	-

	d	4	15	-38.8	-	143.2	-
	d	3	20	-39.4	-0.9	171.6	1.56
	e	4	15	-37.7	0.0	150.3	0.00
	e	3	33	-35.6	-2.6	176.8	4.31
	e	3	30	-39.0	-	143.2	-
	e	4	10	-36.0	-2.4	180.2	4.00
	f	4	15	-37.3	-1.7	165.0	2.88
	f	3	20	-40.9	-1.6	191.2	2.72
	f	4	15	-40.4	-1.6	194.5	2.72
	f	4	25	-41.5	-1.5	175.6	2.56
MEN6-2b	a	3	20	-40.6	-1.0	164.5	1.72
	a	3	20	-42.8	-3.0	111.2	4.93
	a	4	25	-41.5	-1.0	187.0	1.72
	a	4	25	-39.4	-0.2	152.2	0.35
	b	3	25	-41.9	-2.9	210.5	4.77
	b	4	33	-38.8	0.0	186.1	0.00
	b	3	25	-43.6	-4.6	139.1	7.26
	d	3	15	-40.1	-0.7	136.9	1.22
	d	4	15	-40.9	-0.5	130.3	0.87
	d	3	15	-41.1	-1.0	128.0	1.72
	d	2	25	-41.2	-2.0	144.3	3.37

1 – Ratio of vapour phase to liquid phase; 2 - T_m = Final melting temperature of ice within fluid inclusion;
3 - T_h = Final homogenization temperature of vapour phase to fluid phase; 4 - T_f = Final freezing temperature of fluid phase

4.3 – Thermometry by Ti-in-quartz and Zr-in-rutile & rutile trace element analysis

Quartz vein mineralization temperatures from Ti-in-Qtz (Table 4) are calculated using the thermometry equation from Thomas et al. (2010), which give a range of 348°C to 680°C. Rutile mineralization temperatures obtained from Zr-in-rutile are calculated based on three sample types; fractured euhedral acicular rutile (Fig. 8c and 8d) preserved in quartz-carbonate (MEN10-2 and MEN40-2a), host rock which has been preserved during vein throttling (MEN42-5a), and host wall rock just beyond the quartz veining (MEN19-8). Temperatures are determined using the thermometry equation from Tomkins, Powell, and Ellis (2007) ranged from 514°C to 681°C. The range of acicular rutile crystals in the quartz-calcite vein is shown in Table 4.

Geochemical trace element analysis was performed on all rutile types, previously mentioned for thermometry measurements. The analysis (Table 3) shows enrichment of W and Sn moving from the sedimentary host rock rutile blebs to the acicular vein rutile, as well as increasing Nb/Ta ratios moving in the same manner (Fig 13 and 14).

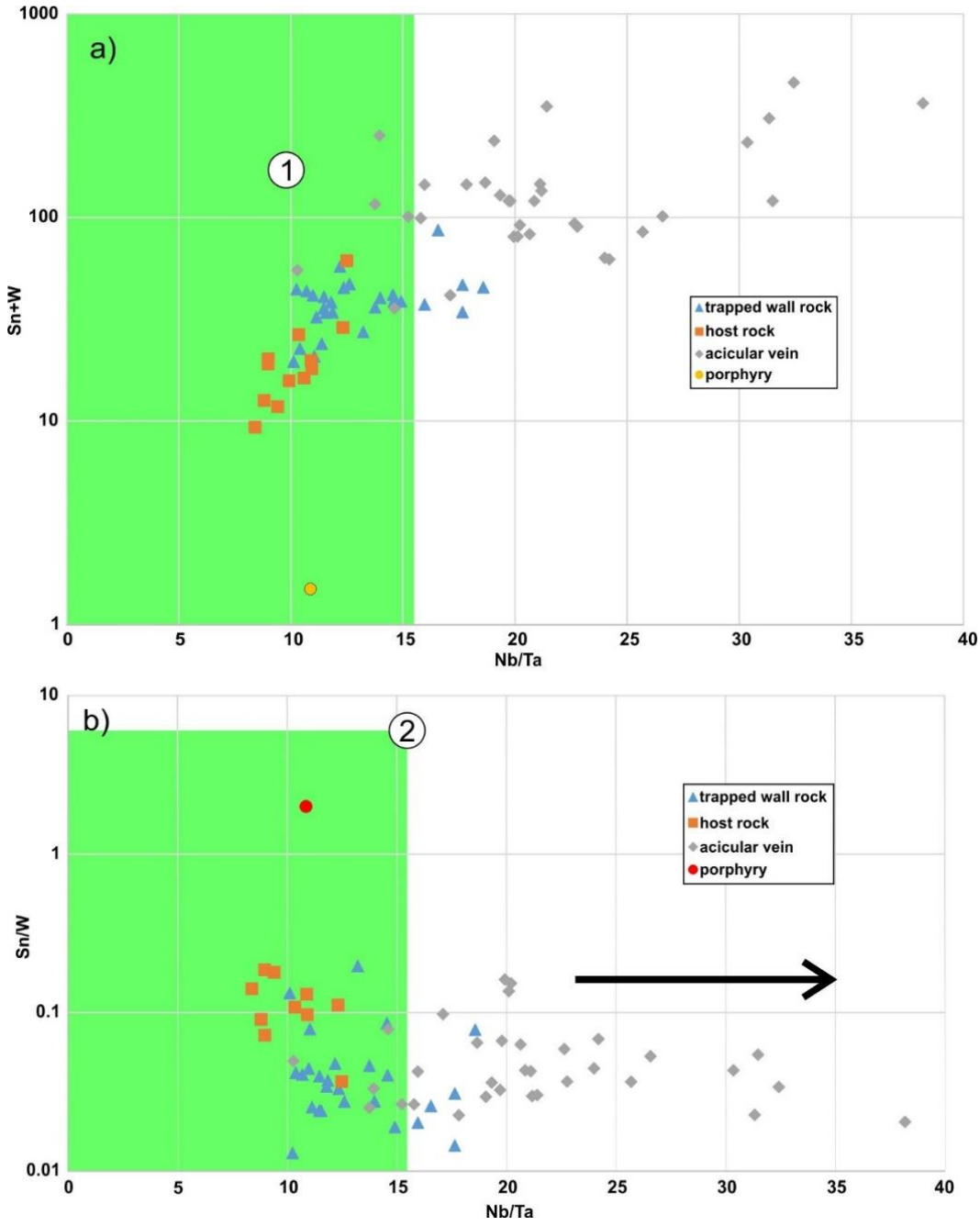

Figure 13 – a) The trace element analysis plotting of Sn+W vs. Nb/Ta for each type of rutile analysis. Field 1: Range of host rock values from bulk rock analysis (Carroll, 2003a) b) Plotted values for Sn/W vs. Nb/Ta for each type of rutile analysis, including a field for bulk rock values of host lithology. Field 2: Range of host rock values from bulk rock analysis (Carroll, 2003a). Note the deviation of values from the host rock lithology for Nb/Ta ratios once measurements move away from the host into the quartz vein as marked by the arrow.

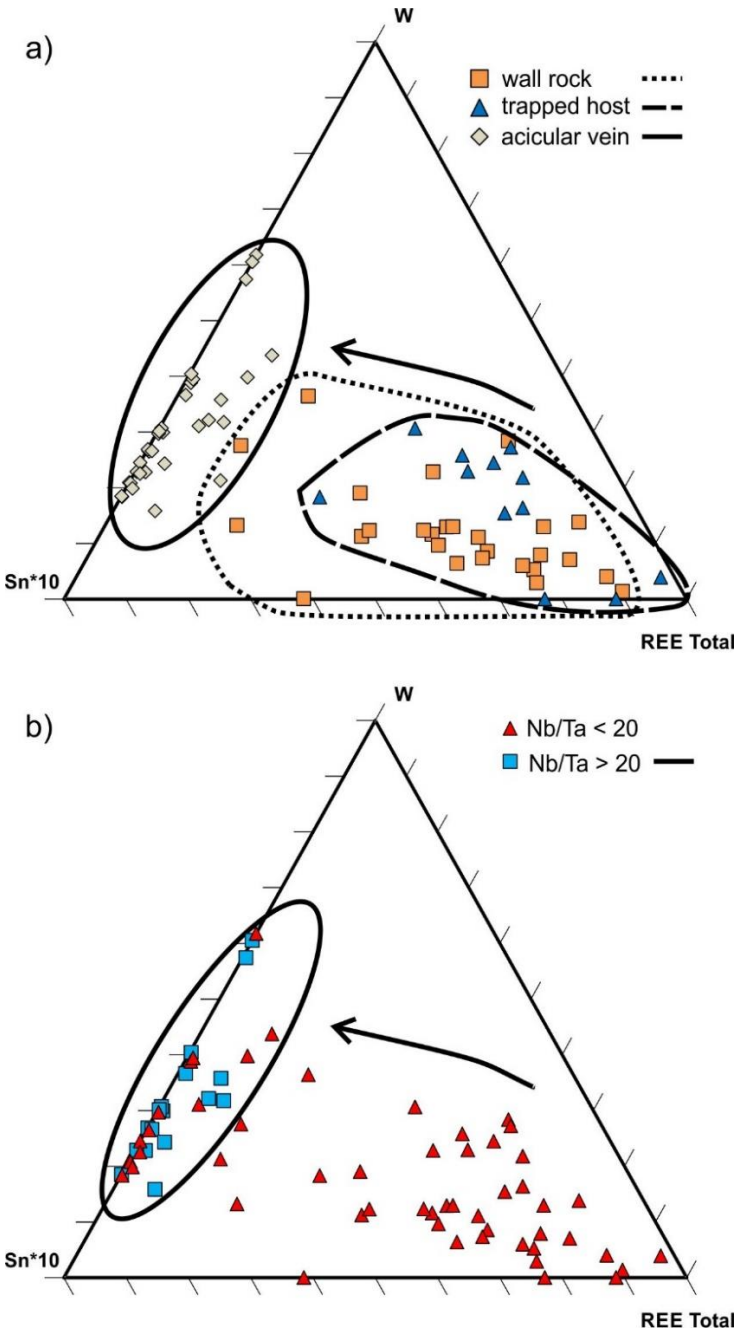

Figure 14 – LA-ICP-MS trace element ternary diagrams. a) Ternary diagram showing abundance of Sn, W, and total REE as represented by rutile host: Wall Rock, Trapped Host, and Acicular Vein. b) Ternary diagram showing the same elements but represented by their Nb/Ta ratios, with the discriminatory value being less than or greater than a ratio of 20, which was chosen arbitrarily. The ratio value was chosen as values greater than 20 are representative of the acicular vein rutile. Note the deviation of data points away from the wall rock towards the acicular vein in 14a as Nb/Ta ratios increase to values above 20 in the same direction, as shown by the arrow in both figures.

Table 3 - LA-ICP-MS trace element data analysis or rutile (ppm)

	Li	Cs	Rb	Ba	Sr	Zr	Hf	Nb	Ta	Th	U	As	Mo	Sb	W	Co	Ni	Cu	Zn	Ga	Sn	La	Ce	Pr	Nd	Y	Sm	Eu	Gd	Tb	Dy	Ho	Er	Tm	Yb	Lu	Pb
Men19-8[1]																																						
2 - 1	17	3.8	84	242	34	144	7.0	1598	155	17	6.7	14	0.0	1.5	24	7.6	28	18	48	11	2.6	3.2	7.4	0.70	3.6	9.8	2.0	0.23	1.7	0.25	2.7	0.48	1.4	0.17	1.1	0.27	37
10-11 - 1	b.d.l	0.44	4.4	24	31	113	4.3	1588	189	4.9	3.9	b.d.l	0.0	1.3	8.2	1.3	2.0	1.7	6.1	1.1	1.2	1.7	5.3	0.69	3.1	12	1.6	0.47	1.8	0.42	2.2	0.37	1.2	0.22	2.0	0.24	4.2
10-11 - 2	b.d.l	0.63	14	40	27	107	3.9	1527	174	8.0	7.5	1.0	0.0	0.80	12	6.0	5.0	1.8	4.4	3.2	1.1	3.1	7.3	0.91	4.9	14	2.4	0.51	2.3	0.45	2.4	0.46	1.5	0.24	1.9	0.21	4.9
1 - 1	b.d.l	0.73	19	67	153	89	5.7	1420	151	27	4.9	b.d.l	1.4	1.2	10	1.3	4.2	b.d.l	14	5.1	1.8	28	93	16	98	82	35	7.7	34	4.4	20	2.8	6.0	0.44	2.3	0.51	2.3
1 - 2	3.0	0.12	36	65	35	115	4.6	1356	137	17	4.7	b.d.l	0.0	0.20	16	1.8	6.8	2.8	16	7.7	b.d.l	13	33	5.0	27	21	5.7	1.4	7.2	0.93	3.9	0.78	2.3	0.27	1.8	0.39	4.2
2 - 1	7.0	0.12	8.5	67	39	122	3.9	1386	131	7.6	6.0	b.d.l	0.0	b.d.l	16	0.41	b.d.l	0.40	7.4	2.5	b.d.l	4.5	8.9	0.95	8.8	17	1.5	0.64	3.3	0.50	4.5	0.68	1.9	0.35	1.8	0.38	3.3
4 - 1	45	11	203	593	135	187	14	1427	116	13	8.2	b.d.l	0.0	0.30	26	15	52	38	84	27	2.9	4.6	8.0	1.5	6.7	18	2.2	0.66	4.8	1.0	4.8	0.47	2.6	0.38	1.9	0.24	16
8 - 1	54	8.4	160	440	40	187	9.8	1453	133	18	5.6	2.0	0.0	0.70	18	18	69	34	120	30	2.3	4.3	10	1.1	6.9	16	2.1	0.44	2.4	0.74	4.2	0.79	1.5	0.44	2.8	0.13	23
8 - 2	47	8.7	109	383	39	157	6.6	1419	130	10	6.9	1.0	0.0	2.4	17	24	88	20	119	21	1.6	2.3	5.2	0.53	4.0	13	1.3	0.38	2.1	0.48	3.5	0.63	1.7	0.19	1.3	0.36	30
9 - 1	31	3.4	61	139	21	221	14	2260	181	9.7	7.8	7.5	0.0	2.4	59	7.4	28	16	37	9.3	2.2	2.1	5.9	0.85	4.2	13	1.0	0.24	1.8	0.51	3.1	0.59	2.0	0.39	2.0	0.23	17
10-11 - 1	17	0.070	9.5	54	29	267	8.9	1527	170	16	9.6	4.6	0.6	0.46	19	1.8	5.7	0.60	14	2.0	1.4	1.9	5.3	0.75	4.3	25	1.9	0.36	2.2	0.57	4.2	0.78	3.6	0.57	3.7	0.64	10
10-11 - 2	0.40	0.90	11	46	45	213	9.4	1579	176	17	11	14	0.1	0.65	16	1.4	8.6	2.7	16	2.1	3.0	4.1	11	1.5	8.2	20	3.1	0.88	3.3	0.56	5.1	0.96	2.2	0.43	2.5	0.42	29
Men42-5a[2]																																						
3 - 1	17	b.d.l	8.3	45	76	259	16	1088	79	21	7.0	13	1.6	3.8	35	13	28	0.50	9.9	3.4	1.6	33	70	7.1	27	21	5.6	1.2	3.8	0.13	3.4	0.27	2.0	0.20	2.4	b.d.l	5.6
3 - 2	6.4	b.d.l	b.d.l	1.9	3.9	209	15	1325	83	1.6	0.75	3.9	b.d.l	0.80	37	b.d.l	b.d.l	1.0	2.6	b.d.l	0.74	2.7	5.0	0.49	1.0	1.3	b.d.l	0.090	0.090	0.080	0.66	b.d.l	0.34	0.090	b.d.l	b.d.l	0.60
3 - 3	1.2	0.0	0.57	11	27	470	16	1181	67	14	6.8	6.7	0.0	b.d.l	45	2.0	b.d.l	1.0	5.2	0.70	1.4	17	34	4.2	15	19	2.7	0.50	2.0	0.52	2.6	0.59	2.4	0.26	3.3	0.45	3.1
3 - 4	b.d.l	0.020	4.0	20	17	243	15	1087	75	3.8	1.8	7.3	0.0	0.0	39	3.0	8.7	b.d.l	8.1	0.90	3.3	2.4	4.4	0.73	3.1	5.3	0.26	0.14	0.97	0.031	0.67	0.030	0.64	0.056	0.31	0.078	2.1
3 - 5	b.d.l	0.020	4.7	17	32	311	21	1968	135	10	3.5	17	0.1	0.40	37	2.0	6.3	2.6	5.9	0.56	1.5	11	22	1.9	8.2	12	1.2	0.22	0.11	0.20	2.3	0.31	2.2	0.14	1.7	0.39	1.8
3 - 6	b.d.l	0.49	4.6	39	79	397	21	1271	72	22	7.3	10	0.0	1.3	34	8.4	7.6	0.90	8.2	2.5	0.49	68	126	15	48	27	7.3	1.9	5.7	0.70	4.9	1.4	3.8	0.41	3.4	0.70	4.8
6 - 1	11	1.3	3.5	17	57	313	19	920	80	11	2.6	3.5	0.0	b.d.l	33	0.20	4.6	1.9	3.5	1.3	0.80	17	41	4.3	15	17	3.3	1.1	3.4	0.57	3.4	0.60	1.6	0.33	1.6	0.27	1.5
6 - 2	7.0	0.84	3.9	24	41	261	12	1560	136	11	4.1	1.0	0.0	b.d.l	35	1.3	6.6	0.70	16	0.94	1.4	5.9	14	2.2	11	24	3.5	1.3	3.8	0.56	4.6	0.85	2.5	0.19	1.3	0.26	1.4
6 - 3	4.0	0.51	5.8	37	61	265	19	1527	149	9.2	3.9	b.d.l	0.0	b.d.l	44	4.4	8.7	2.4	10	2.3	0.57	29	56	6.6	27	13	3.3	0.80	2.0	0.35	2.5	0.50	1.6	0.16	2.0	0.25	2.6
6 - 4	b.d.l	0.12	2.6	5.1	14	196	9.6	1240	109	4.6	1.7	8.0	0.0	b.d.l	24	0.84	6.3	0.90	6.9	1.1	b.d.l	1.2	3.8	0.48	1.8	4.7	0.44	0.0	0.060	0.048	0.71	0.12	0.64	0.13	0.92	0.040	0.38
7 - 1	21	4.5	81	238	88	260	15	1528	151	24	13	13	0.2	5.7	17	29	31	35	56	13	2.3	18	41	4.0	20	22	2.8	0.69	4.5	0.45	4.4	0.71	3.1	0.22	4.3	0.47	16
7 - 2	5.5	0.23	3.3	22	40	281	20	1652	134	8.4	4.2	17	0.0	2.1	44	5.3	4.0	8.8	b.d.l	0.75	1.5	12	22	2.4	9.9	11	1.6	0.17	1.9	0.22	1.7	0.55	1.2	0.12	1.3	0.13	3.4
7 - 3	2.6	0.32	3.7	18	32	233	21	1900	173	5.7	2.4	5.6	0.0	1.0	40	1.9	1.9	1.7	5.1	0.58	1.8	4.1	9.4	0.89	6.1	8.1	1.4	0.38	0.79	0.14	1.6	0.38	0.73	0.14	0.97	0.17	3.2
7 - 4	5.6	0.16	b.d.l	2.3	9.9	640	19	1860	125	26	10	7.8	0.0	0.34	38	0.21	b.d.l	0.40	11	0.11	0.72	3.4	6.6	1.1	3.0	34	0.65	0.28	1.4	0.28	3.9	1.2	4.0	0.66	5.9	1.3	2.0
4-5 - 1	6.5	0.62	23	50	7.7	273	17	2111	173	5.7	3.5	0.20	1.6	0.57	55	1.8	5.5	1.9	10	2.3	2.6	0.28	1.3	0.34	1.1	6.5	b.d.l	b.d.l	0.63	b.d.l	0.89	0.020	1.3	0.31	0.98	0.31	3.2
8-9 - 1	8.0	0.31	8.0	29	32	101	4.1	901	81	6.7	4.0	2.7	3.1	1.5	32	1.8	15	0.50	15	1.2	0.80	7.8	22	3.1	17	6.5	4.5	b.d.l	3.3	0.27	2.4	b.d.l	1.3	b.d.l	1.3	0.12	0.7
8-9 - 2	8.0	1.5	14	34	34	141	6.4	1074	94	10	9.2	7.0	0.4	b.d.l	40	1.4	24	0.40	21	3.4	1.0	1.2	4.1	0.29	4.9	13	2.7	0.010	2.3	0.48	3.0	0.53	1.8	0.23	1.1	0.19	2.4
3 - 1	4.3	b.d.l	1.9	13	30	338	15	1011	54	7.8	2.9	9.9	0.0	0.90	42	0.67	2.2	1.8	4.8	0.40	3.3	9.5	21	2.3	13	11	3.0	0.62	2.2	0.32	2.2	0.55	1.5	0.16	1.4	0.25	1.8
3 - 2	23	5.1	125	312	42	243	15	2083	158	17	9.7	19	1.9	3.0	23	22	48	4.6	12	14	4.5	18	37	4.0	9.4	13	1.8	0.41	0.99	0.47	2.0	0.54	1.3	0.050	1.7	0.16	12
6 - 1	11	0.15	2.0	9.5	22	580	26	1608	150	31	11	2.7	0.0	2.1	42	2.0	8.2	1.3	12.5	1.5	1.7	20	52	4.8	21	32	2.4	0.89	4.0	0.47	4.7	1.0	3.9	0.96	7.2	0.88	2.5
6 - 2	0.7	0.31	0.88	6.0	22	305	18	1399	111	4.6	1.9	6.4	0.0	1.4	46	0.53	4.5	2.2	7.4	0.79	1.3	8.3	15	2.0	7.2	5.7	1.3	0.26	0.88	0.18	1.7	0.31	0.78	0.064	0.47	0.056	1.1
7 - 1	2.8	1.6	20.0	51	36	257	15	1587	144	12	6.0	b.d.l	0.0	1.8	19	2.4	10	8.9	15	3.5	1.5	14	28	3.2	12	13	2.3	0.82	1.6	0.43	2.5	0.49	1.8	0.25	2.2	0.20	8.7
7 - 3	b.d.l	0.59	3.8	29	91	228	16	1335	113	11	2.4	8.2	0.0	0.32	33	5.7	4.5	0.80	5.4	1.6	1.2	59	120	12	41	13	3.7	0.66	4.5	0.48	2.3	0.54	1.9	0.19	0.81	0.14	3.7
7 - 4	6.4	0.44	0.97	9.7	28	395	16	1022	73	12	6.1	3.8	0.0	1.6	39	1.8	3.4	2.6	5.1	0.68	1.1	6.5	14	1.9	8.9	18	2.3	0.51	2.1	0.39	2.3	0.56	1.8	0.29	2.0	0.40	3.2
7 - 5	4.6	b.d.l	0.33	5.9	29	284	22	1830	155	6.5	1.5	2.0	0.0	1.2	37	0.38	2.4	2.1	3.1	0.30	1.3	8.9	22	2.2	8.6	6.4	1.2	0.21	0.54	0.13	0.74	0.26	0.47	0.20	1.2	0.13	1.7
4-5 - 1	7.0	0.18	1.8	5.1	149	700	24	1628	98	31	14	8.3	0.0	2.5	85	1.5	7.2	1.7	9.2	0.98	2.2	20	50	8.0	43	66	16	3.2	16	2.13	13.9	2.6	7.0	1.1	7.3	1.1	3.8
8-9 - 1	7.5	0.22	13	42	33	152	8.1	834	80	8.3	5.4	2.2	0.0	2.3	22	2.5	13	0.90	11	2.7	0.91	2.1	5.2	0.54	6.4	13	1.4	0.56	2.2	0.44	3.3	0.56	1.7	0.26	1.3	0.34	1.9

1 - Host rock; 2 - Trapped host rock in quartz vein

Table 3 Cont. - LA-ICP-MS trace element data analysis or rutile (ppm)

	Li	Cs	Rb	Ba	Sr	Zr	Hf	Nb	Ta	Th	U	As	Mo	Sb	W	Co	Ni	Cu	Zn	Ga	Sn	La	Ce	Pr	Nd	Y	Sm	Eu	Gd	Tb	Dy	Ho	Er	Tm	Yb	Lu	Pb
Men10-2[3]																																						
1	4.0	b.d.l	b.d.l	2.2	3.5	173	13	1912	99	3.1	3.6	b.d.l	b.d.l	b.d.l	124	0.071	2.5	b.d.l	2.5	0.29	4.5	0.045	0.21	0.025	0.17	0.30	0.0	b.d.l	b.d.l	b.d.l	0.0	b.d.l	b.d.l	b.d.l	b.d.l	b.d.l	0.49
2	5.4	b.d.l	b.d.l	16	12	124	7.0	1456	85	9.4	5.9	3.0	b.d.l	2.2	38	0.26	1.2	b.d.l	4.0	0.090	3.7	1.3	2.7	0.28	0.98	2.5	0.20	0.31	0.51	0.034	0.56	0.11	0.066	0.034	0.22	b.d.l	1.2
3	2.7	b.d.l	0.15	0.70	5.6	193	15	1150	62	0.40	0.22	b.d.l	b.d.l	1.0	140	b.d.l	b.d.l	0.60	1.3	0.11	9.0	0.22	0.69	0.082	0.46	0.70	0.0	0.037	b.d.l	0.026	0.041	0.060	b.d.l	b.d.l	0.050	b.d.l	0.32
4	b.d.l	0.12	0.20	9.8	15	162	13	1184	60	0.24	0.33	12	b.d.l	0.30	113	b.d.l	b.d.l	0.50	7.3	0.018	7.5	0.58	0.86	0.14	0.12	0.20	0.0	b.d.l	b.d.l	b.d.l	0.0	b.d.l	0.085	b.d.l	b.d.l	b.d.l	0.69
5	b.d.l	b.d.l	0.24	4.1	9.6	180	16	1220	59	0.94	0.39	16	b.d.l	b.d.l	116	0.042	0.60	2.7	b.d.l	b.d.l	5.0	0.41	0.65	0.060	0.32	0.081	0.0	0.12	b.d.l	b.d.l	0.0	b.d.l	b.d.l	b.d.l	b.d.l	b.d.l	0.64
6	b.d.l	0.090	0.34	3.5	11	314	23	3865	181	1.2	0.20	17	b.d.l	0.0	341	0.16	1.3	b.d.l	6.3	b.d.l	10	0.93	2.3	0.27	0.95	1.9	0.32	0.23	0.35	0.10	0.42	0.059	b.d.l	0.008	0.042	b.d.l	4.9
7	b.d.l	0.15	b.d.l	b.d.l	0.89	83	5.9	1563	103	0.0	0.30	23	b.d.l	b.d.l	98	0.058	1.8	1.5	4.1	0.22	2.6	b.d.l	0.070	b.d.l	b.d.l	b.d.l	0.0	b.d.l	b.d.l	b.d.l	0.0	b.d.l	b.d.l	b.d.l	b.d.l	b.d.l	1.2
8	b.d.l	0.11	0.25	0.11	1.6	297	20	1785	100	0.0	0.32	5.9	b.d.l	0.30	142	0.019	0.80	4.1	4.3	b.d.l	3.2	b.d.l	0.11	b.d.l	b.d.l	0.056	0.0	0.067	b.d.l	b.d.l	0.090	b.d.l	b.d.l	b.d.l	b.d.l	b.d.l	0.69
9	b.d.l	0.020	0.26	2.0	3.0	474	27	3809	189	0.0	0.46	6.0	b.d.l	b.d.l	71	0.049	0.80	4.6	2.8	0.037	9.7	0.15	0.38	0.019	b.d.l	0.23	0.0	0.10	0.070	b.d.l	0.038	b.d.l	b.d.l	b.d.l	b.d.l	b.d.l	0.66
10	2.1	b.d.l	b.d.l	0.10	0.58	514	27	3976	199	0.0	0.23	0.40	b.d.l	0.70	69	0.18	b.d.l	b.d.l	1.6	0.14	11	b.d.l	b.d.l	b.d.l	b.d.l	b.d.l	0.0	b.d.l	b.d.l	b.d.l	0.043	b.d.l	b.d.l	b.d.l	b.d.l	b.d.l	0.51
11	1.2	b.d.l	b.d.l	b.d.l	0.78	515	25	4067	201	0.0	0.29	3.2	b.d.l	1.4	80	0.16	0.70	b.d.l	6.0	0.35	12	b.d.l	b.d.l	b.d.l	b.d.l	b.d.l	0.0	b.d.l	b.d.l	b.d.l	0.0	b.d.l	b.d.l	b.d.l	b.d.l	b.d.l	0.57
12	b.d.l	b.d.l	0.09	0.12	4.7	74	7.2	3340	138	0.31	0.017	8.7	b.d.l	0.30	58	b.d.l	b.d.l	b.d.l	2.1	b.d.l	4.0	0.087	0.19	b.d.l	b.d.l	b.d.l	0.0	b.d.l	b.d.l	b.d.l	0.0	b.d.l	b.d.l	b.d.l	b.d.l	b.d.l	0.51
13	1.4	0.13	b.d.l	b.d.l	0.93	160	13	1280	56	0.32	0.028	1.3	b.d.l	0.30	87	0.18	b.d.l	b.d.l	1.7	0.12	3.2	0.013	b.d.l	b.d.l	b.d.l	0.090	0.0	b.d.l	b.d.l	b.d.l	0.0	b.d.l	b.d.l	b.d.l	b.d.l	b.d.l	0.45
14	2.7	b.d.l	b.d.l	2.0	4.2	85	6.7	2117	82	2.0	0.15	b.d.l	b.d.l	2.5	82	0.069	0.40	7.8	10	0.080	3.0	0.029	0.22	b.d.l	b.d.l	0.53	0.0	0.081	0.05	b.d.l	0.0	b.d.l	0.090	b.d.l	b.d.l	b.d.l	0.43
15	b.d.l	0.060	b.d.l	1.5	4.9	96	7.7	2189	91	1.2	0.10	4.2	b.d.l	0.40	61	0.056	0.80	0.50	3.8	0.090	2.7	0.11	0.20	b.d.l	b.d.l	0.021	0.0	b.d.l	b.d.l	b.d.l	0.0	b.d.l	b.d.l	b.d.l	b.d.l	b.d.l	0.51
16	2.4	0.060	0.38	0.17	1.8	181	15	1383	65	0.03	b.d.l	6.3	b.d.l	0.10	131	0.059	0.60	0.20	2.0	b.d.l	3.9	0.12	0.32	b.d.l	b.d.l	0.068	0.0	b.d.l	b.d.l	b.d.l	0.0	b.d.l	b.d.l	b.d.l	b.d.l	b.d.l	0.61
17	5.0	0.080	0.22	b.d.l	0.52	206	17	1254	64	0.0	b.d.l	11	b.d.l	0.0	117	0.068	0.40	1.9	1.7	b.d.l	3.8	b.d.l	b.d.l	b.d.l	b.d.l	b.d.l	0.0	b.d.l	b.d.l	b.d.l	0.0	b.d.l	b.d.l	b.d.l	b.d.l	b.d.l	0.27
18	0.3	b.d.l	b.d.l	2.2	4.2	125	11	2428	107	0.0	0.46	4.7	b.d.l	b.d.l	88	0.030	1.3	b.d.l	7.3	0.11	5.2	0.42	0.97	0.042	0.26	0.091	0.0	b.d.l	b.d.l	b.d.l	0.070	b.d.l	b.d.l	b.d.l	b.d.l	b.d.l	0.55
19	1.5	0.010	0.54	0.78	2.6	92	9.5	2139	134	0.0	0.20	6.2	b.d.l	0.90	139	0.064	0.70	b.d.l	6.3	0.24	5.9	0.17	0.44	0.022	0.11	b.d.l	0.0	b.d.l	b.d.l	b.d.l	0.0	b.d.l	b.d.l	b.d.l	b.d.l	b.d.l	0.53
20	7.0	0.38	1.0	33	85	1196	75	1219	87	23	5.4	b.d.l	b.d.l	1.0	244	0.40	2.3	b.d.l	6.0	0.42	8.1	7.9	16	1.9	8.3	11	1.4	1.1	1.7	0.33	2.2	0.47	1.3	0.23	1.3	0.24	5.9
1 - 1	b.d.l	b.d.l	0.13	b.d.l	1.5	120	n.a.	n.a.	n.a.	0.045	0.17	n.a.	n.a.	n.a.	n.a.	n.a.	n.a.	n.a.	n.a.	0.088	n.a.	n.a.	n.a.	n.a.	n.a.	0.049	n.a.	n.a.	n.a.	n.a.	n.a.	n.a.	n.a.	n.a.	n.a.	n.a.	0.012
1 - 2	0.2	0.067	0.54	1.3	8.4	537	n.a.	n.a.	n.a.	10	2.9	n.a.	n.a.	n.a.	n.a.	n.a.	n.a.	n.a.	n.a.	0.12	n.a.	n.a.	n.a.	n.a.	n.a.	0.80	n.a.	n.a.	n.a.	n.a.	n.a.	n.a.	n.a.	n.a.	n.a.	n.a.	0.25
2 - 1	2.5	0.13	0.082	11	5.7	183	n.a.	n.a.	n.a.	0.56	0.36	n.a.	n.a.	n.a.	n.a.	n.a.	n.a.	n.a.	n.a.	0.15	n.a.	n.a.	n.a.	n.a.	n.a.	0.18	n.a.	n.a.	n.a.	n.a.	n.a.	n.a.	n.a.	n.a.	n.a.	n.a.	0.21
2 - 2	b.d.l	0.020	0.055	2.3	9.0	194	n.a.	n.a.	n.a.	0.58	0.12	n.a.	n.a.	n.a.	n.a.	n.a.	n.a.	n.a.	n.a.	0.12	n.a.	n.a.	n.a.	n.a.	n.a.	0.30	n.a.	n.a.	n.a.	n.a.	n.a.	n.a.	n.a.	n.a.	n.a.	n.a.	0.24
2 - 3	b.d.l	b.d.l	0.017	2.9	9.6	189	n.a.	n.a.	n.a.	3.3	2.1	n.a.	n.a.	n.a.	n.a.	n.a.	n.a.	n.a.	n.a.	0.11	n.a.	n.a.	n.a.	n.a.	n.a.	0.99	n.a.	n.a.	n.a.	n.a.	n.a.	n.a.	n.a.	n.a.	n.a.	n.a.	0.48
2 - 4	2.1	0.057	b.d.l	4.9	6.0	78	n.a.	n.a.	n.a.	1.5	1.2	n.a.	n.a.	n.a.	n.a.	n.a.	n.a.	n.a.	n.a.	0.19	n.a.	n.a.	n.a.	n.a.	n.a.	0.25	n.a.	n.a.	n.a.	n.a.	n.a.	n.a.	n.a.	n.a.	n.a.	n.a.	0.35
3 - 1	b.d.l	0.11	0.070	2.4	0.86	543	n.a.	n.a.	n.a.	0.0	0.38	n.a.	n.a.	n.a.	n.a.	n.a.	n.a.	n.a.	n.a.	0.18	n.a.	n.a.	n.a.	n.a.	n.a.	0.080	n.a.	n.a.	n.a.	n.a.	n.a.	n.a.	n.a.	n.a.	n.a.	n.a.	0.35
3 - 2	b.d.l	0.0020	0.011	0.01	0.86	536	n.a.	n.a.	n.a.	0.0	0.36	n.a.	n.a.	n.a.	n.a.	n.a.	n.a.	n.a.	n.a.	0.063	n.a.	n.a.	n.a.	n.a.	n.a.	0.048	n.a.	n.a.	n.a.	n.a.	n.a.	n.a.	n.a.	n.a.	n.a.	n.a.	0.017
3 - 3	b.d.l	0.016	0.021	0.01	5.0	482	n.a.	n.a.	n.a.	0.0	0.53	n.a.	n.a.	n.a.	n.a.	n.a.	n.a.	n.a.	n.a.	0.037	n.a.	n.a.	n.a.	n.a.	n.a.	0.17	n.a.	n.a.	n.a.	n.a.	n.a.	n.a.	n.a.	n.a.	n.a.	n.a.	0.11
3 - 4	b.d.l	0.033	b.d.l	1.4	2.5	377	n.a.	n.a.	n.a.	0.0	0.20	n.a.	n.a.	n.a.	n.a.	n.a.	n.a.	n.a.	n.a.	0.070	n.a.	n.a.	n.a.	n.a.	n.a.	0.24	n.a.	n.a.	n.a.	n.a.	n.a.	n.a.	n.a.	n.a.	n.a.	n.a.	0.047
4 - 1	b.d.l	0.082	0.054	0.81	3.8	74	n.a.	n.a.	n.a.	0.25	0.03	n.a.	n.a.	n.a.	n.a.	n.a.	n.a.	n.a.	n.a.	0.071	n.a.	n.a.	n.a.	n.a.	n.a.	0.16	n.a.	n.a.	n.a.	n.a.	n.a.	n.a.	n.a.	n.a.	n.a.	n.a.	0.12
4 - 2	1.4	0.036	0.07	3.4	6.8	102	n.a.	n.a.	n.a.	1.0	0.23	n.a.	n.a.	n.a.	n.a.	n.a.	n.a.	n.a.	n.a.	0.078	n.a.	n.a.	n.a.	n.a.	n.a.	0.43	n.a.	n.a.	n.a.	n.a.	n.a.	n.a.	n.a.	n.a.	n.a.	n.a.	0.30
4 - 3	0.0	0.065	0.097	5.0	5.7	90	n.a.	n.a.	n.a.	0.37	0.065	n.a.	n.a.	n.a.	n.a.	n.a.	n.a.	n.a.	n.a.	0.071	n.a.	n.a.	n.a.	n.a.	n.a.	0.23	n.a.	n.a.	n.a.	n.a.	n.a.	n.a.	n.a.	n.a.	n.a.	n.a.	0.33
4 - 4	0.7	b.d.l	0.077	3.3	7.0	137	n.a.	n.a.	n.a.	0.29	0.018	n.a.	n.a.	n.a.	n.a.	n.a.	n.a.	n.a.	n.a.	0.28	n.a.	n.a.	n.a.	n.a.	n.a.	0.060	n.a.	n.a.	n.a.	n.a.	n.a.	n.a.	n.a.	n.a.	n.a.	n.a.	0.28
5 - 1	9.7	0.046	2.1	1.5	4010	289	n.a.	n.a.	n.a.	3.5	0.87	n.a.	n.a.	n.a.	n.a.	n.a.	n.a.	n.a.	n.a.	1.1	n.a.	n.a.	n.a.	n.a.	n.a.	71	n.a.	n.a.	n.a.	n.a.	n.a.	n.a.	n.a.	n.a.	n.a.	n.a.	0.80
5 - 2	35	0.16	0.35	26	1270	283	n.a.	n.a.	n.a.	2.5	2.8	n.a.	n.a.	n.a.	n.a.	n.a.	n.a.	n.a.	n.a.	0.56	n.a.	n.a.	n.a.	n.a.	n.a.	35	n.a.	n.a.	n.a.	n.a.	n.a.	n.a.	n.a.	n.a.	n.a.	n.a.	0.25
5 - 3	12	0.14	3.7	12	733	229	n.a.	n.a.	n.a.	3.0	0.97	n.a.	n.a.	n.a.	n.a.	n.a.	n.a.	n.a.	n.a.	1.5	n.a.	n.a.	n.a.	n.a.	n.a.	22	n.a.	n.a.	n.a.	n.a.	n.a.	n.a.	n.a.	n.a.	n.a.	n.a.	0.49

3 - Acicular rutile crystals in quartz-carbonate vein

Table 3 Cont. - LA-ICP-MS trace element data analysis or rutile (ppm)

	Li	Cs	Rb	Ba	Sr	Zr	Hf	Nb	Ta	Th	U	As	Mo	Sb	W	Co	Ni	Cu	Zn	Ga	Sn	La	Ce	Pr	Nd	Y	Sm	Eu	Gd	Tb	Dy	Ho	Er	Tm	Yb	Lu	Pb
Men40-2a[4]																																						
1	41	0.090	b.d.l	11	14	766	74	501	49	3.3	2.1	2.8	b.d.l	1.6	53	0.38	b.d.l	9.6	11	0.16	2.6	0.44	1.4	0.18	0.47	2.2	0.0	0.097	0.09	0.015	0.049	0.014	0.22	b.d.l	b.d.l	b.d.l	0.50
2	6.1	0.14	b.d.l	0.59	3.4	279	30	1437	91	0.52	0.33	7.4	b.d.l	0.20	97	0.014	b.d.l	b.d.l	6.3	0.20	2.6	0.074	0.26	0.0080	b.d.l	0.047	0.0	b.d.l	b.d.l	b.d.l	0.0	b.d.l	b.d.l	b.d.l	b.d.l	b.d.l	0.16
3	4.5	b.d.l	0.05	2.0	4.0	85	5.1	1444	105	0.14	0.32	13	b.d.l	b.d.l	114	0.15	0.50	b.d.l	13	b.d.l	2.9	0.13	0.51	0.043	b.d.l	0.50	0.0	0.041	b.d.l	b.d.l	0.080	b.d.l	0.12	b.d.l	0.18	b.d.l	0.11
4	7.5	b.d.l	b.d.l	5.5	15	184	14	2540	133	0.58	0.36	7.1	b.d.l	b.d.l	231	0.10	1.7	b.d.l	6.0	b.d.l	6.8	0.62	0.88	0.16	0.28	0.74	0.0	0.15	b.d.l	b.d.l	0.21	b.d.l	b.d.l	b.d.l	b.d.l	b.d.l	0.35
5	b.d.l	b.d.l	0.07	4.6	115	248	33	1531	58	2.6	0.88	b.d.l	b.d.l	b.d.l	96	0.13	0.30	2.4	4.9	0.23	5.1	1.2	2.6	0.36	2.0	3.2	0.60	0.17	0.39	0.14	0.58	0.16	0.11	0.064	b.d.l	b.d.l	0.67
6	b.d.l	b.d.l	0.38	3.4	40	183	27	2790	89	1.1	1.2	b.d.l	b.d.l	0.40	114	0.12	1.2	8.5	5.7	b.d.l	6.2	1.2	3.7	0.49	3.0	5.6	0.96	0.45	0.80	0.072	1.6	0.26	0.64	0.008	0.46	0.0070	0.54
7	3.3	b.d.l	0.34	14	273	332	26	2517	66	3.4	1.1	15	b.d.l	1.4	357	0.070	2.2	4.1	6.5	0.11	7.3	2.5	4.6	0.74	4.6	11	0.53	0.98	1.8	0.40	1.5	0.62	0.78	0.20	0.76	0.11	0.55
8	165	2.9	52	109	45	205	20	2585	80	9.6	4.8	6.4	b.d.l	2.7	445	0.97	8.5	1.1	40	8.3	15	2.3	4.7	0.98	4.4	6.3	1.19	0.48	1.2	0.32	1.6	0.15	0.59	0.16	0.68	0.037	2.1
9	9.5	0.12	0.06	0.97	3.7	357	29	2860	94	0.49	0.49	b.d.l	b.d.l	b.d.l	224	0.17	b.d.l	2.7	7.2	b.d.l	9.7	0.076	0.35	0.018	0.16	0.27	0.06	b.d.l	b.d.l	0.008	0.0	b.d.l	b.d.l	b.d.l	b.d.l	b.d.l	0.33
10	12	0.090	0.15	2.4	2.5	106	11	2610	83	0.15	0.15	b.d.l	b.d.l	b.d.l	300	0.14	1.4	1.4	4.1	b.d.l	6.8	0.023	0.13	b.d.l	b.d.l	0.054	0.0	0.034	b.d.l	b.d.l	0.0	b.d.l	b.d.l	b.d.l	b.d.l	b.dl	0.24
11	1.4	0.13	b.d.l	24	19	181	14	1423	69	15	3.2	b.d.l	b.d.l	1.4	78	0.071	0.20	b.d.l	7.0	0.090	4.9	0.95	2.4	0.25	1.3	2.9	0.37	0.78	0.12	0.025	0.63	0.12	0.25	b.d.l	0.041	0.031	1.9
12	b.d.l	0.030	b.d.l	11	10	98	7.4	1266	87	6.7	1.8	4.1	b.d.l	2.0	33	0.29	b.d.l	4.8	12	0.032	2.6	1.1	1.4	0.22	0.71	1.6	0.22	0.21	0.23	0.055	0.22	0.008	0.17	b.d.l	0.24	0.040	2.1
1 - 1	17	0.18	14	20	351	313	n.a.	n.a.	n.a.	11	3.4	n.a.	n.a.	n.a.	n.a.	n.a.	n.a.	n.a.	n.a.	1.6	n.a.	n.a.	n.a.	n.a.	n.a.	31	n.a.	n.a.	n.a.	n.a.	n.a.	n.a.	n.a.	n.a.	n.a.	n.a.	2.7
1 - 2	9.4	1.3	0.06	84	555	142	n.a.	n.a.	n.a.	7.4	1.6	n.a.	n.a.	n.a.	n.a.	n.a.	n.a.	n.a.	n.a.	0.44	n.a.	n.a.	n.a.	n.a.	n.a.	28	n.a.	n.a.	n.a.	n.a.	n.a.	n.a.	n.a.	n.a.	n.a.	n.a.	0.84
1 - 3	0.50	0.13	0.19	13	104	73	n.a.	n.a.	n.a.	1.8	0.55	n.a.	n.a.	n.a.	n.a.	n.a.	n.a.	n.a.	n.a.	0.24	n.a.	n.a.	n.a.	n.a.	n.a.	8.8	n.a.	n.a.	n.a.	n.a.	n.a.	n.a.	n.a.	n.a.	n.a.	n.a.	0.60
1 - 4	3.7	0.089	1.2	13	95	319	n.a.	n.a.	n.a.	1.8	1.6	n.a.	n.a.	n.a.	n.a.	n.a.	n.a.	n.a.	n.a.	0.32	n.a.	n.a.	n.a.	n.a.	n.a.	9.6	n.a.	n.a.	n.a.	n.a.	n.a.	n.a.	n.a.	n.a.	n.a.	n.a.	0.39
2 - 1	b.d.l	0.020	0.081	11	4.7	131	n.a.	n.a.	n.a.	0.20	0.11	n.a.	n.a.	n.a.	n.a.	n.a.	n.a.	n.a.	n.a.	0.034	n.a.	n.a.	n.a.	n.a.	n.a.	0.34	n.a.	n.a.	n.a.	n.a.	n.a.	n.a.	n.a.	n.a.	n.a.	n.a.	0.14
2 - 2	b.d.l	0.015	b.d.l	1.4	1.9	266	n.a.	n.a.	n.a.	0.16	0.18	n.a.	n.a.	n.a.	n.a.	n.a.	n.a.	n.a.	n.a.	0.044	n.a.	n.a.	n.a.	n.a.	n.a.	0.024	n.a.	n.a.	n.a.	n.a.	n.a.	n.a.	n.a.	n.a.	n.a.	n.a.	0.089
2 - 3	b.d.l	b.d.l	0.033	0.13	2.3	579	n.a.	n.a.	n.a.	0.04	0.019	n.a.	n.a.	n.a.	n.a.	n.a.	n.a.	n.a.	n.a.	0.043	n.a.	n.a.	n.a.	n.a.	n.a.	0.052	n.a.	n.a.	n.a.	n.a.	n.a.	n.a.	n.a.	n.a.	n.a.	n.a.	0.068
2 - 4	2.1	0.046	0.20	0.71	1460	662	n.a.	n.a.	n.a.	0.56	0.55	n.a.	n.a.	n.a.	n.a.	n.a.	n.a.	n.a.	n.a.	0.091	n.a.	n.a.	n.a.	n.a.	n.a.	7.9	n.a.	n.a.	n.a.	n.a.	n.a.	n.a.	n.a.	n.a.	n.a.	n.a.	0.21
3 - 1	b.d.l	0.038	0.56	20	6.6	272	n.a.	n.a.	n.a.	3.1	1.2	n.a.	n.a.	n.a.	n.a.	n.a.	n.a.	n.a.	n.a.	b.d.l	n.a.	n.a.	n.a.	n.a.	n.a.	6.0	n.a.	n.a.	n.a.	n.a.	n.a.	n.a.	n.a.	n.a.	n.a.	n.a.	0.48
3 - 2	b.d.l	b.d.l	b.d.l	6.0	7.7	231	n.a.	n.a.	n.a.	0.56	0.050	n.a.	n.a.	n.a.	n.a.	n.a.	n.a.	n.a.	n.a.	0.10	n.a.	n.a.	n.a.	n.a.	n.a.	0.22	n.a.	n.a.	n.a.	n.a.	n.a.	n.a.	n.a.	n.a.	n.a.	n.a.	0.45
4 - 1	0.30	b.d.l	0.25	5.0	3.0	223	n.a.	n.a.	n.a.	0.49	0.47	n.a.	n.a.	n.a.	n.a.	n.a.	n.a.	n.a.	n.a.	0.071	n.a.	n.a.	n.a.	n.a.	n.a.	2.5	n.a.	n.a.	n.a.	n.a.	n.a.	n.a.	n.a.	n.a.	n.a.	n.a.	0.17
4 - 2	b.d.l	0.094	0.071	3.8	0.72	266	n.a.	n.a.	n.a.	0.0	0.45	n.a.	n.a.	n.a.	n.a.	n.a.	n.a.	n.a.	n.a.	0.075	n.a.	n.a.	n.a.	n.a.	n.a.	0.019	n.a.	n.a.	n.a.	n.a.	n.a.	n.a.	n.a.	n.a.	n.a.	n.a.	0.067
4 - 3	1.4	b.d.l	0.65	b.d.l	5.0	233	n.a.	n.a.	n.a.	0.57	0.87	n.a.	n.a.	n.a.	n.a.	n.a.	n.a.	n.a.	n.a.	0.23	n.a.	n.a.	n.a.	n.a.	n.a.	0.87	n.a.	n.a.	n.a.	n.a.	n.a.	n.a.	n.a.	n.a.	n.a.	n.a.	0.20
5 - 1	0.90	0.043	0.087	3.2	13	396	n.a.	n.a.	n.a.	3.8	1.3	n.a.	n.a.	n.a.	n.a.	n.a.	n.a.	n.a.	n.a.	0.14	n.a.	n.a.	n.a.	n.a.	n.a.	2.0	n.a.	n.a.	n.a.	n.a.	n.a.	n.a.	n.a.	n.a.	n.a.	n.a.	0.96
5 - 2	2.3	0.019	0.08	12	15	150	n.a.	n.a.	n.a.	9.4	1.8	n.a.	n.a.	n.a.	n.a.	n.a.	n.a.	n.a.	n.a.	0.12	n.a.	n.a.	n.a.	n.a.	n.a.	1.7	n.a.	n.a.	n.a.	n.a.	n.a.	n.a.	n.a.	n.a.	n.a.	n.a.	2.3
5 - 3	1.7	0.029	1.1	20	12	188	n.a.	n.a.	n.a.	7.9	2.2	n.a.	n.a.	n.a.	n.a.	n.a.	n.a.	n.a.	n.a.	0.17	n.a.	n.a.	n.a.	n.a.	n.a.	3.4	n.a.	n.a.	n.a.	n.a.	n.a.	n.a.	n.a.	n.a.	n.a.	n.a.	3.4

4 - acicular rutile crystal in quartz-carbonate vein; n.a. = not available; b.d.l. = below detection level

Table 4 - Zr and Ti LA-ICP-MS values from rutile and quartz, respectively

Sample/ Analysis #	Zr (ppm)	T(°C)$_1$	Sample	Ti (ppm)	T(°C)$_2$
Men10-2			Men10-2		
1 - 1	120	546	1 - 1	44	482
1 - 2	537	658	1 - 2	59	505
2 - 1	183	575	2 - 1	32	459
2 - 2	194	579	2 - 2	83	533
2 - 3	189	577			
2 - 4	77.5	518			
3 - 1	543	659	3 - 1	99	549
3 - 2	536	658	3 - 2	14.5	406
3 - 3	482	649			
3 - 4	377	629			
4 - 1	74.2	515	4 - 1	9.6	382
4 - 2	102	535	4 -2	45	484
4 - 3	90.1	527			
4 - 4	137	554			
5 - 1	289	608			
5 - 2	283	606			
5 - 3	229	591			
Men40-2a			Men40-2a		
1 - 1	313	614	1 - 1	91	541
1 - 2	142	557	1 - 2	28	449
1 - 3	72.7	514	2 - 0	350	680
1 - 4	319	616			
2 - 1	131	551	2 - 1	100	550
2 - 2	266	602	2 - 2	77	527
2 - 3	579	665	3 - 0	25	441
2 - 4	662	676			
3 - 1	272	603	3 - 1	33	461
3 - 2	231	591	3 - 2	5.1	348
4 - 1	223	589	4 - 1	7.9	371
4 - 2	266	602	4 - 2	6.6	361
4 - 3	233	592			
5 - 1	396	633			
5 - 2	150	561			
5 - 3	188	576			

Temperatures calculated with assumed pressure of P = 1kbar.
Calculations from: 1 - Tomkins, Powell, and Ellis (2007);
2 - Thomas et al. (2010)

4.4 – Vein quartz textures and generations

A single sample showing visible electrum, a Maisie quartz grab sample (Fig. 5, 15, and 16), was used for CL analysis. Variations in colour indicate compositional variations within the quartz. The Maisie quartz sample shows small colour variations, as well as a lineated

clast from the host rock (Fig. 15b). The quartz colour is red-purple, with small variation in colour shading. This is not a strong enough variation to indicate major compositional or isotopic changes within the quartz. The minor variation in colour is enough to warrant SIMS analysis of the Maisie quartz sample and host clast within, to determine what the isotopic makeup of both are.

4.5 – Oxygen isotope systematics of vein quartz

Twenty measurements using SIMS gave $\delta^{18}O_{V\text{-}SMOW}$ values ranging from 12.3 – 18.8‰ (Fig. 15a), with an average value of 15.6 ± 1.9‰. This range of $\delta^{18}O_{V\text{-}SMOW}$ paired with the temperatures from Ti-in-quartz thermometry gives a calculated (Faure & Mensing, 2005) initial fluid isotope value ranging from 7 – 18.5‰ (Fig. 17) that would result in the final isotope values determined from SIMS.

4.6 - Laser Raman microscopy/spectroscopy

For the liquid composition curve the spectra returns peaks for nitrogen, methane, and water. The 0wt% NaCl and 5.5wt% NaCl curves in Mernagh and Wilde (1989) best match the curve present in Figure 18. Based off of analysis from Mernagh and Wilde (1989) the shape of the water peak is consistent with that of a low salinity fluid, which is supported by the fluid inclusion microthermometry performed.

The vapour curve spectra (Fig. 18) returns peaks for nitrogen, methane, and water. The nitrogen and methane peaks are larger and more distinct than those from the liquid curve, as they are from direct measurement, instead of background noise from the fluid.

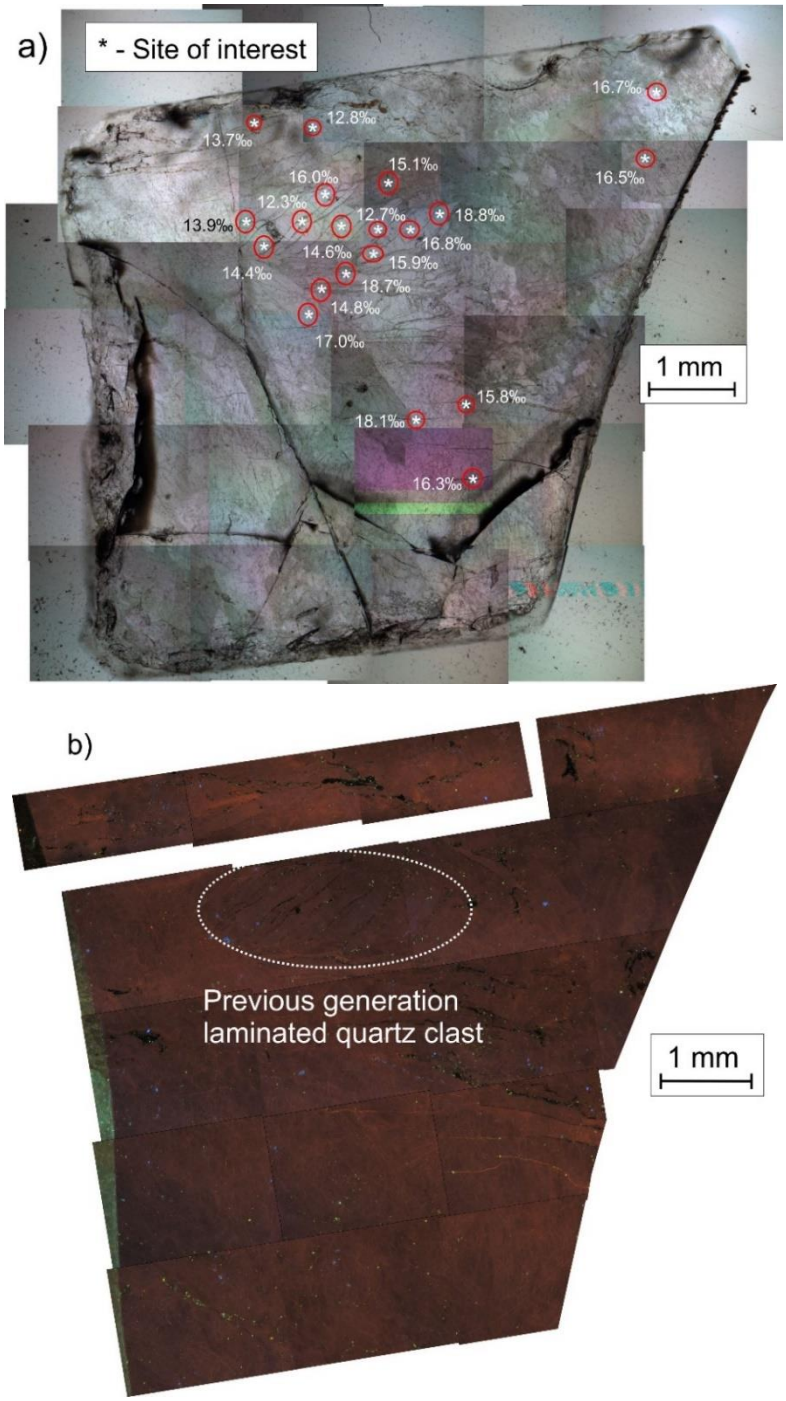

Figure 15 – Maisie quartz chips from Maisie quartz sample (Fig. 5a). a) Transmitted light image of Maisie quartz chip showing sites of SIMS analysis for $\delta^{18}O$. A total $\delta^{18}O$ variation of ~6.5‰ is seen from SIMS measurements. b) Cathodoluminescence image of the same chip, showing colour variations representing potential different quartz generations, which guided the selection process for sites of interest from 15a. Previous generation of quartz shown with laminated quartz clast present in the chip.

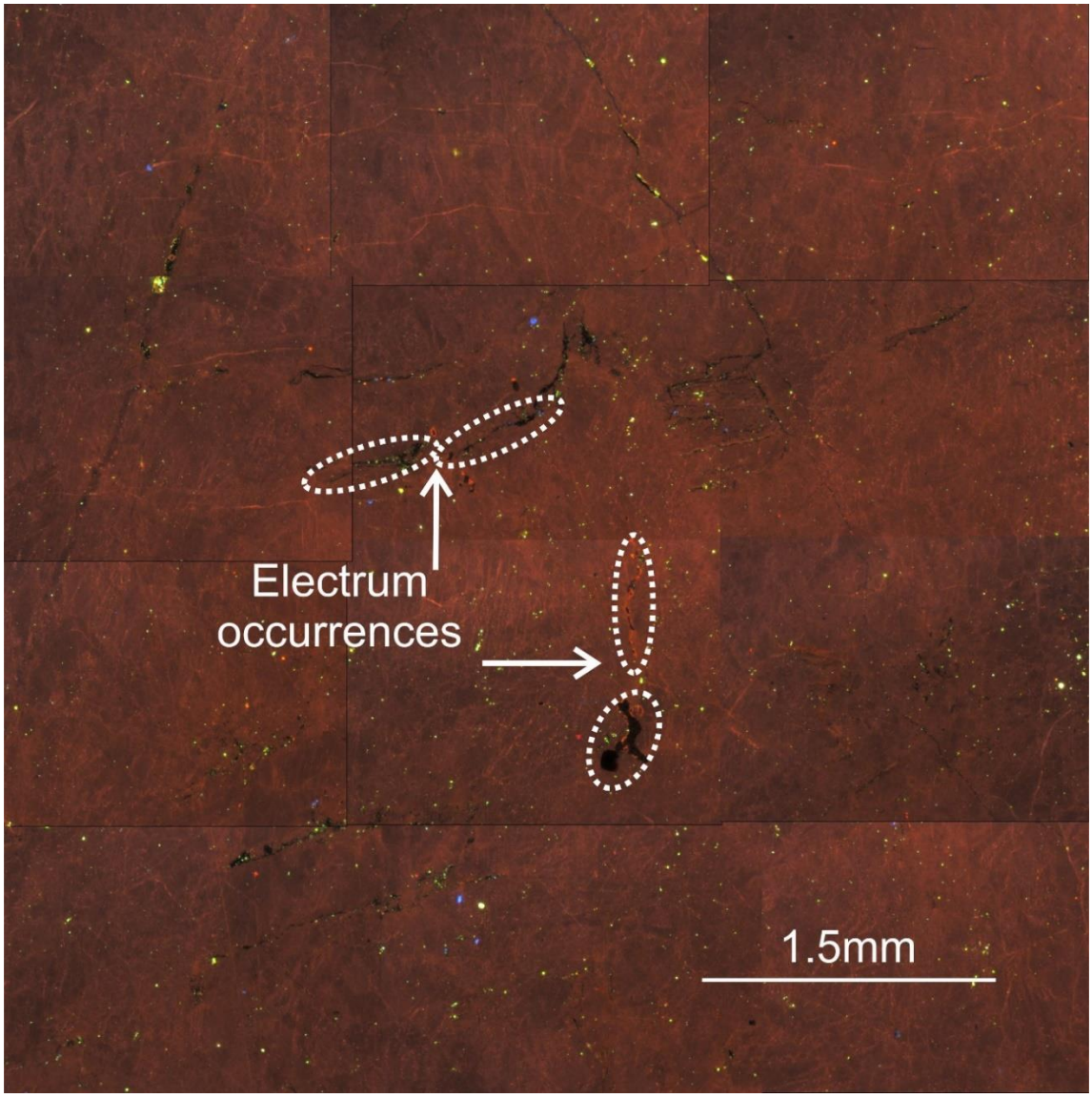

Figure 16 – CL quartz vein from Maisie. Image is the magnified boxed area (b) from Fig. 5. Areas with electrum mineralization are circled. Electrum can be seen associated with fractured blacked out areas in this sample, which were holes in the thin section or hematite/ pyrite.

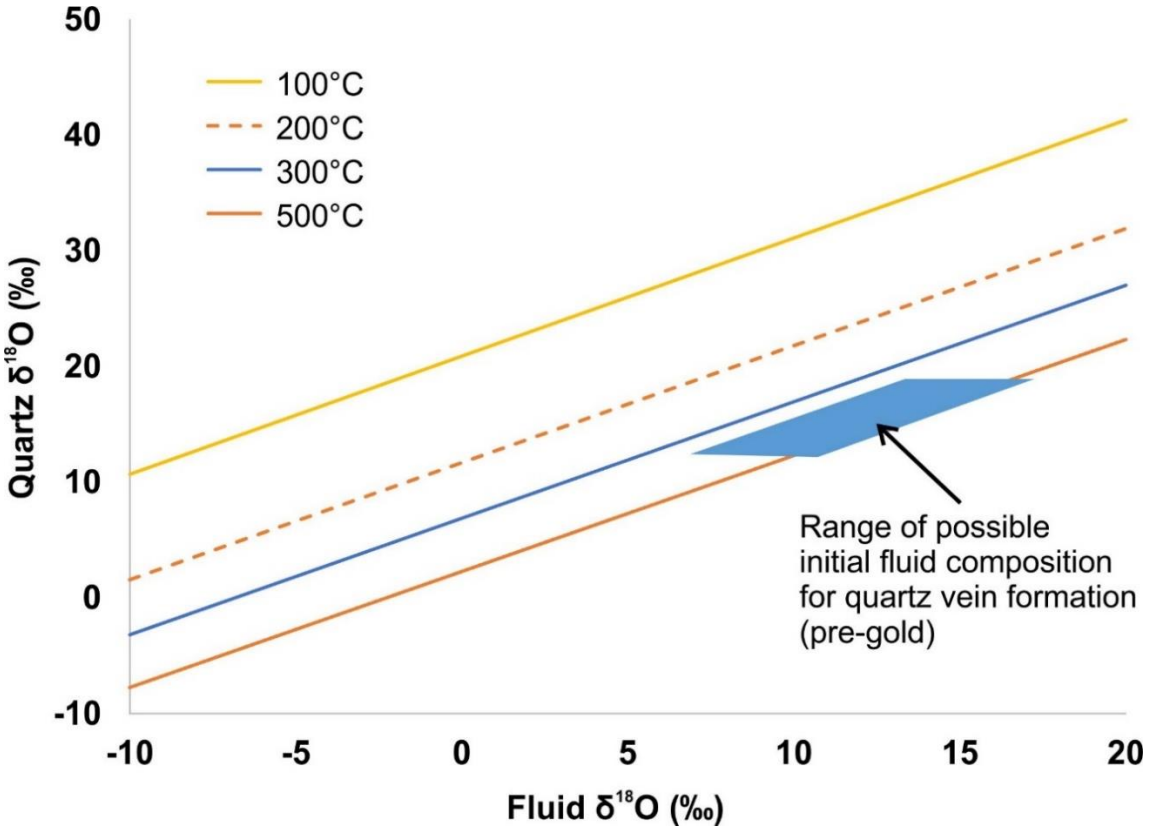

Figure 17 – Oxygen isotope modeling of initial isotopic value required to precipitate quartz with final measured values of $\delta^{18}O_{V\text{-}SMOW}$. Quartz $\delta^{18}O$ values are from SIMS analysis of Maisie quartz chip (Fig. 15), with fluid $\delta^{18}O$ values constrained by the temperatures calculated from Ti-in-quartz thermometry (Table 4). Temperature lines were created using equations from Faure and Mensing, 2005, and Sharp and Kirschner, 1994, and inputting data points from Table 2 & 4.

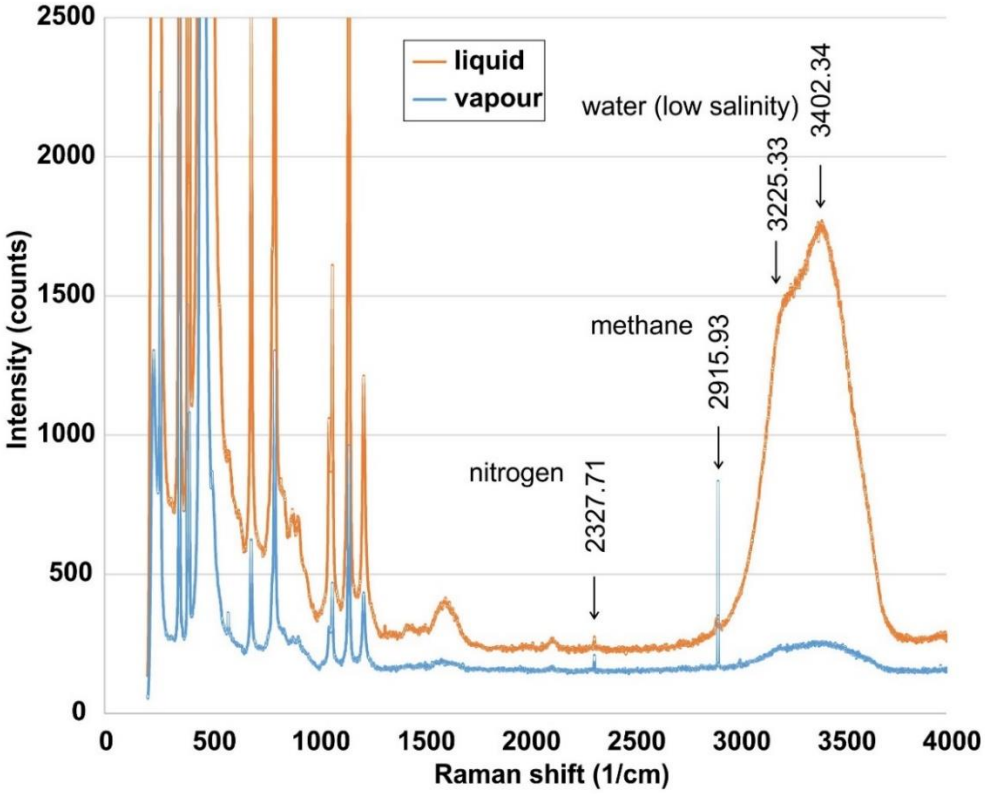

Figure 18 – Laser Raman spectra for liquid and vapour phases in fluid inclusions from quartz sample Men5.

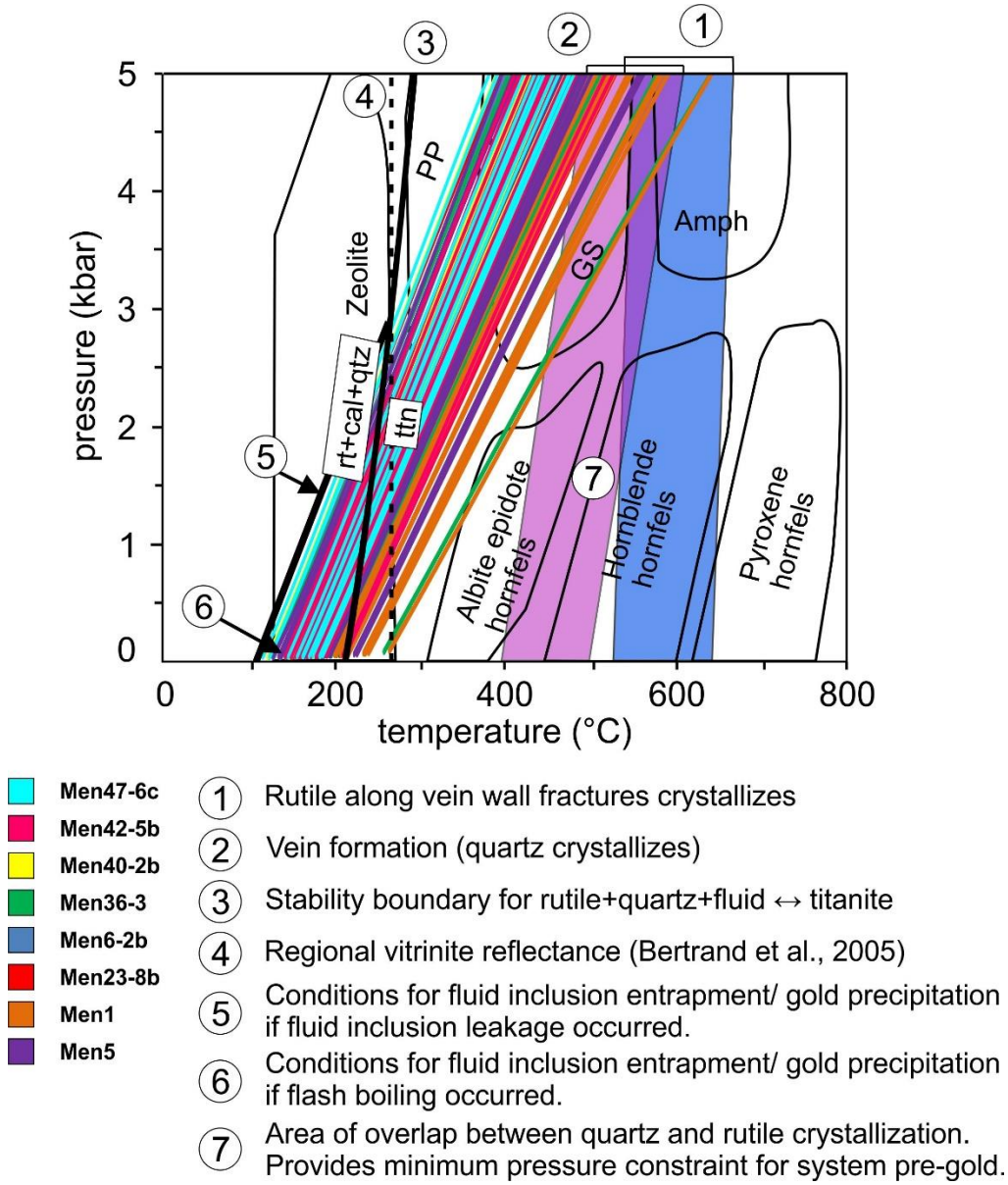

Figure 19 – Isochores for all Maisie fluid inclusions. 1 – Temperature range calculated from Zr in rutile (Table 4). 2 – Temperature range calculated from Ti in quartz vein (Table 4). 3 – Stability line for rutile and titanite. The field to the left of the line is rutile stable, and titanite stability to the right of the line. 4 – Maximum temperature from vitrinite reflectance for the area. 5 – Field of stability for formation of fluid inclusions and rutile, showing the range of PT given a minimum value of entrapment if leakage has occurred. 6 – Field of stability for formation of fluid inclusions during flash boiling, resulting in abundant vapour-rich fluid inclusions. 7 – Area where quartz and rutile crystallization overlaps. This area represents a minimum pressure constrain on the system pre-gold deposition. The system would need to undergo ~1.5kbar of decompression to achieve the boiling conditions necessary for gold deposition.

5.0 Discussion

5.1 – Pressure-temperature constraints on fluid entrapment and gold deposition

Fluid inclusion petrography found secondary quartz-hosted inclusions. Based on textural evidence, the gold precipitation at the Maisie showing appears to be late stage, post-dating quartz veins, infilling vugs and fractures within the veins. Therefore, secondary fluids may be ore forming fluids.

The first thermal event to occur at the Maisie deposit was the growth of acicular rutile grains (Field 1, Fig. 19). Evidence for this is the textural relationship between acicular vein rutile and the quartz-calcite veining. The quartz-calcite is shown infilling the fractured rutile crystals as seen in Figures 8c and 8d. The rutile crystals grew in open space, forming euhedral acicular grains along the quartz vein walls, and as the quartz vein grow around them, the rutile crystals were plucked from the wall and incorporated into the Maisie quartz vein. Evidence for the timing of this event is the temperatures reported from the Zr-in-rutile thermometry for acicular vein rutile, which range from 514 – 676 °C (Table 4). The lack of visible zircon in the system means one of two things. First, zircon has yet to be observed and is fully buffering the system. The other option is if there is no crystalline zircon in the system, so what Zr is being partitioned into other minerals has a lower activity and the thermometer acts as a maximum temperature range. Based on the temperatures reported from rutile and quartz analysis, the area locally around the Maisie quartz vein would have been much higher temperature than peak temperature of regional metamorphism. Gold precipitation is controlled by a number of factors, but for this system there are likely two main controls. Gold precipitates either during cooling of the system when gold in solution

becomes insoluble and drops out, or when sulphide mineralization occurs decreasing the sulphur content in solution, as gold solubility is controlled by sulphur content in the system. Therefore prior to gold precipitation, the hydrothermal system would have to cool down to lower temperature, or have large amounts of sulphide mineralization. However, there is little sulphide mineralization, so the primary control would be temperature. This data is not restricted to only one section of the Maisie quartz vein, as samples for thermometry were selected along multiple sections of the quartz vein. These sections range from areas adjacent to the porphyry (Men 10) and further to the north east of the Maisie quartz vein (Men 40) as seen in Figure 2. The two sites of analysis are separated by ~200 m, with values that show little deviation in their temperatures and Zr content (Table 4). Additional trace element data for the rutile shows that the system is homogeneous and unique, as the trace element signatures for Sn, W, Nb, and Ta all group in similarly plotted regions (Fig. 13, Table 3). These values are unique to the Maisie vein as well, as values sit isolated from outside host rock rutile and trapped host rock in quartz-calcite vein rutile (Fig. 14). Though these rutile analyses constrain initial temperature conditions for the hydrothermal system, they provide little information for the pressure. For all thermometric calculations, a pressure of 1 kbar was assumed; however, pressures could be different from that in the system.

The next thermal event to occur is the precipitation of first generation quartz veining. The quartz precipitating at this point in time occurred at temperatures of 348-680 °C (based on the Thomas et al. (2010) thermometer, Table 4). Based on isochore modelling (Fig. 19, Fields 5 and 6), electrum in mineralizing at temperatures of ~100 – 250 °C. The

temperatures for early quartz crystallization then are too high for electrum mineralization to occur, meaning early quartz is barren. Texturally the quartz is pre-gold precipitation, as it forms vugs and cracks that are later infilled by electrum (Fig. 8a/b and 9). Temperature of the electrum forming events are further constrained by these events, but pressure is still undefined in this system.

Pressure has little variation based on Figure 19, ranging from 0 – 1.5 kbar. The minimum pressure of the system pre-gold, is shown by Field 7 (Fig. 19), where the temperature fields of quartz and rutile crystallization intersect. The lowest point of intersection (Field 7, Fig. 19) of ~1.5 kbar represents a minimum pressure constraint for the system. For electrum mineralization the system would then have to undergo that much decompression, and drop to lower pressures. The pressure is also assumed to be low in the system as the quartz veins and sedimentary host rocks contain no high pressure metamorphic minerals (Fig. 19). There are no high grade metamorphic minerals present in the surrounding host rocks of Maisie. The only metamorphic mineral present is biotite (Fig. 8d). Further supporting the low grade metamorphism in the area is the “hot” CL showing that quartz is a dark shade of red to light purple in places (Fig. 16). These colours occur with low grade metamorphic events, whereas higher grade metamorphic events give quartz colours of dark purple to blue (Boggs et al., 2002). The pressure of the system is less easily constrained. There are two pressure fields that would explain the system. If decrepitation has occurred in the system then most inclusions in the samples are empty with only a few rare surviving two phase inclusions. This would result in isochores that constrain the temperature and pressure to the field in Figure 19 (Field 5). If the system is the result of

flash boiling, the temperature cannot be higher than the L+V curve (Fig. 19, Field 6) for a fluid with the measured salinities of this study.

As the hydrothermal system continues to cool, secondary fluid inclusions begin to be entrapped in the Maisie quartz vein. In this study, two types of fluid inclusions are observed; rare 2-phase (liquid-vapour) inclusions (Fig. 10, type I), and more common monophase inclusions. Monophase inclusions appear to either be empty or contain only low density vapour. In the former case, inclusions may have opened allowing their contents to escape, rendering microthermometric measurements irrelevant. In the latter case, if not decrepitated, an explanation is needed for the predominance of vapour inclusions with rare two phase inclusions. Isochores show a PT range of ~100 - 210°C and ~0 – 3kbar based on isochores and the rutile+calcite+quartz ↔ titanite stability line (Field 3, Fig. 19). To differentiate between either the high pressure zone for electrum mineralization (Field 5, Fig. 19) or low pressure mineralization (Field 6, Fig. 19), further evidence of boiling or deformation must be observed.

Box-and-whisker plots for homogenization temperatures (Fig. 11) show real fluctuation in P-T conditions of the system. The distribution of error bars or "whiskers" shows the typical range that occurs during flash-boiling of the system or leakage/ decrepitation of inclusions. The small variation in P-T could be caused by pressure throttling during crack-seal events which would result in leakage of the inclusions. Variation may also be caused from under or over pressure during exhumation or faulting, which is observed in the area of the APA.

Fluid inclusion homogenization temperatures indicate that electrum deposition is late stage as temperatures from rutile and initial quartz precipitation (Table 4) are much higher than that of the homogenization temperatures (Table 2, Fig. 19 - Fields 5 and 6). Along with homogenization temperatures, the low temperatures reported from vitrinite reflectance of the regional host rocks (Bertrand and Malo, 2005) indicates that quartz veining occurred post- regional metamorphism. This can be seen by the early stage quartz veining having much higher temperatures (Table 4) locally than regionally. These initial high temperatures show that electrum would not have been deposited at the same time as the vein reached its maximum temperatures, as rutile and quartz vein temperatures would overprint the region and remobilize the gold in solution. The hydrothermal system would then need to cool down before gold would fall out of solution.

The stability boundary for rutile+quartz+calcite ↔ titanite (Castelli et al, 2007) (Field 3, Fig. 19) constrains the maximum temperature of entrapment for the fluid inclusions as well as gold deposition. This reaction boundary is valid, despite rutile growing initially at much higher temperatures, beyond that which rutile would be stable with calcite. When high temperature early vein rutile formed there had been no associated carbonate phase at that point, meaning the reaction from Castelli et al (2007) would not apply, allowing rutile to form freely. Rutile is now stable with calcite present, as it sits in a lower temperature regime, indicating calcite is post rutile, and late stage in the system.

5.2 – *Fluid source*

Given P-T conditions (Fig. 19) and calculated $\delta^{18}O_{V\text{-}SMOW}$ (Fig. 17), the $\delta^{18}O$ values of 7 – 18.5‰ indicate a potential fluid source being magmatic, formational, metamorphic

in origin, or a mixture of the various fluids. This is supported by little variation in fluid salinity (Fig. 12), high isotope values (Fig. 17), and little variation in quartz isotope values within a sample (Fig. 15).

Low variance in salinities (Fig. 12) indicates little to no fluid mixing, which would result in a larger spread of data. The consistent low salinity values and little flux rules out meteoric waters as a source. If the fluids were meteoric the salinity would be lower, near 0 ‰, and if meteoric mixing occurred then there would be much greater range in the reported salinities. One anomalous sample, Men40-2b assemblage 'b', shows a higher range in salinity of 0.35 – 18.46 eq. wt% NaCl (Fig. 12). This is from four measure inclusions, with two inclusions giving salinities above 10 eq. wt% NaCl. This very small data set is likely an outlier, coming from a data set of 150 fluid inclusion microthermometric measurements.

The elevated $\delta^{18}O$ values may be from the regional metamorphism of the Menneval area, with sediments releasing fluids during dehydration. This would match with isotope fields for metamorphic sedimentary fluids, which sit in higher isotopic range. The source of the sedimentary fluids is not yet known. The immediate sediments of the Grog Brook surrounding the Maisie vein could have an impact, with the introduction of the adjacent porphyry mobilizing fluids in the region. More likely though are deeper source sediments that are being metamorphosed during regional tectonism.

Though not exposed in the APA, Balmoral Group rocks may underlie the Grog Brook Group and may in part be the source material for the Grog Brook sedimentary rocks. Like the sedimentary rocks of the Grog Brook Group, Balmoral Group rocks are somewhat elevated in gold. Unpublished data (R.A. Wilson), shows that 17 of 26 samples collected

have gold contents greater then detection limits (2 ppb). Of these, the average gold content is 14 ppb with a range from 2 to 32 ppb.

While Raman spectroscopy identified methane and nitrogen as the vapour phase, there was no visible CO_2 peak (Fig. 18). It is uncharacteristic for a system to have no visible CO_2, as most gold deposit types report ~3 – 15 mol.% CO_2 (Goldfarb et al., 2005) . The apparent lack of CO_2 may be explained by fractionation during flash-boiling whereby the CO_2 entered the empty looking type II inclusions (Fig. 10). These inclusions were not measured due to their empty appearance, but it is possible that they are vapour rich and contain CO_2.

5.3 – Trace element discrimination of rutile

The results from rutile LA-ICP-MS show an increasing Nb/Ta ratio in samples as they move from host rock outside the quartz vein, then to host rock trapped in the quartz vein, and finally the acicular rutile grains in the Maisie veins (Fig. 13 and 14). Additionally, there is an increase in Sn and W in samples as they move from the host sediment to the Maisie quartz vein. Acicular vein rutile is depleted in everything but W, Sn, the HFSE's (Nb, Ta, Zr, Hf), and show a minor enrichment in As. These unique trace signatures as seen in Table 3 and Figures 13/14 show that the Maisie vein rutile is different from rutile in the surrounding host sediments.

The database from Carroll (2003a) shows no lithologies with Nb/Ta ratios as high as values measured from laser ablation. These values would then be caused from fluid fractionation, with Nb able to travel more efficiently than Ta, leaving Ta behind in the host lithology. This behavior of enriched Nb and fluid fractionation also occurs in the mantle

during subduction related melting (Meinhold, 2010). Future work will include searching through the sedimentary host for depleted Nb or enriched Ta to find the host that would be sourcing the Nb/Ta and potentially the gold.

5.4 – Comparison of Maisie to other orogenic systems

Orogenic gold deposit as described by Groves et al. (1998), Goldfarb et al. (2001, 2005), Robert (1996), and Kerrich and Wyman (1990) are characterized by a number of criteria. The first is the age of the deposits. The Maisie occurrence is hosted by Middle to Late Ordovician clastic sediments. Orogenic deposits span from the Middle Archean to the Tertiary. In Canada, orogenic deposits tend to exist in four major age groups: Late Archean, Early Proterozoic, Cambrian-Ordovician, and Triassic-Jurassic (Robert, 1996). In New Brunswick the dominant age of orogenic deposits is Ordovician.

The terrains most associated with orogenic deposits are transpressional to compressional structures, and they are also in association with metamorphic terrains. The metamorphic grades in the areas tend to be low grade greenschist, though they can get as high as lower-amphibolite, such as in the Contwoyto Lake region in Nunavut (Robert, 1996). Metamorphic grades higher than these tend to keep gold in solution, preventing gold deposition. Additional regions that are similar to these conditions are Goldenville, Nova Scotia; Red Lake, Ontario; and San Antonia, Manitoba to list a few.

Orogenic deposits generally have a set deposit mineralogy consisting of sulphide minerals such as pyrite, pyrrhotite, chalcopyrite, and arsenopyrite, with an ore metal signature of Au-Ag ± As-B-Bi-Sb-Te-W. The existing sulphide minerals are characterized by a low sulphide content of ≤ 3-5% Fe-sulphide, with ≤ 5-15% carbonate minerals/phases.

Gange minerals generally are quartz, ankerite, calcite, dolomite, siderite, and cholorite to name a few.

Finally, large orogenic events with deep seated faults will have mineralizing fluids ranging in temperatures of ~200-600°C. The local vitrinite reflectance of the Menneval area (Bertrand et al, 2005) however does not match these higher end temperatures, putting an initial constraint on the mineralizing fluids temperature. The pressure constraint on these mineralizing fluids do vary with depth, whether they are epizonal (<6 km), mesozonal (6-12km), or hypozonal (>12km) deposits (Groves et al, 1998), which are all classifications based on the depth of emplacement. Additionally, the fluids associated with orogenic deposits are uniformly low fluid salinities of <3 wt% NaCl equivalent, CO_2 fluid contents of 5-30 mol%, and spatial association with major faults.

Before the 2011 discovery of the quartz-vein hosted free electrum in the Lavoie-Maisie electrum occurrences by Tim Lavoie and Mike Taylor respectively, four other metallic mineral occurrences were recognized in the area, including the Fe-Cu ± Au sulphide skarn mineralization associated with intermediate to felsic intrusions at McKenzie Gulch (Lentz et al., 1995), the poly-metallic (Cu ± Zn-Pb etc.) sulphides associated with the Patapedia skarn system (Lentz et al., 1995), the Ritchie Brook Cu-skarn occurrences, and the Manzer Giberson Cu-Ag quartz vein system, though these last two occurrences are poorly located and unsubstantiated historical reports of mineralization in the vicinity of the Lavoie prospect. Since then the Lavoie-Menneval area has gained increased interest in exploration potential, in particular the Menneval region, which is the larger and more studied of the two regions, with an extensive drilling program having occurred in the Menneval region.

While being located in the same structural regime as existing deposits, the Maisie deposit does not share the same deposit mineralogy as other deposits in northwestern New Brunswick. Based on the results found through petrography, microanalysis, and comparison to other previously mentioned New Brunswick deposit types, the system at Maisie appears to be an epizonal-orogenic deposit. Evidence of boiling, as found by fluid inclusion microthermometry, supports a shallow depth of emplacement for the deposit, only occurring at ~ 0.5 – 1.0 kbar. Fluid inclusion microthermometry and Raman spectroscopy/spectrometry found the fluids to be low salinity, which suggests a lack of mixing with deeper hydrothermal fluids/brines. The accessory minerals are sulphide minerals, which are common in orogenic systems, however the low abundance and lack of association with arsenopyrite or pyrrhotite, which is more common in shallow systems, is unique to Maisie.

5.6 – Future research questions

Further detailed CL is needed to determine the variance in quartz compositions. The detailed CL will then lead into further SIMS analysis of quartz, as well as SIMS of calcite in regions with quartz-calcite in equilibrium to determine an additional thermometer.

Further LA-ICP-MS of sulphides present in the quartz vein will be done to determine if similar elemental enrichment and depletions are occurring in other minerals, or if it is unique to the Ti bearing minerals.

The occurrence of Ti bearing minerals in the adjacent porphyry is yet to be examined in detail, and how they relate to both the Ti bearing minerals in the Maisie quartz

vein and surrounding host rock. The relation of potential magmatic fluids from the porphyry and electrum mineralization will be further studied.

Dating of the porphyry has still not been fully determined, and monazite geochronological dating will be used to determine this.

A gas chromatograph crush will be performed to determine hydro-carbon content and gas composition of Maisie quartz-calcite vein samples.

6.0 Conclusions

The study at Maisie has helped to characterize and better understand the electrum showing in the area. Ore and vein petrography found free electrum hosted in quart-calcite veining, in close association to hematitized pyrite in fractures and open spaces. Accessory sulphide minerals in the quartz-calcite vein are pyrite (which is commonly hematitized), with lesser galena, and sphalerite. Other accessory minerals are rutile, monazite, and apatite. Trace element analysis of the rutile in quartz veins found an enrichment of Sn, W, and REE's (notably Ta and Nb). These enrichments occur only rutile in the quartz-calcite veining, and drop to standard background levels within rutile of the host rocks. LA-ICP-MS analysis of the quartz and rutile gave two thermometers, a Zr-in-rutile thermometer giving temperatures of 514 – 676°, and a Ti-in-quartz thermometer giving temperatures of 348-680°C. Fluid inclusion microthermometry and petrography identified two different inclusion phases: (i) rare two phase liquid-vapour inclusions and (ii) common "empty" single phase inclusions. The "empty" phases appear to be a vapour rich phase caused by boiling in the hydrothermal system during gold precipitation, which is thought to be the main mechanism at the time. Rare two phase liquid-vapour inclusions are small (4 ± 1µm

on average) and have homogenization temperatures of 170.3 ± 30.8°C (1σ) on average, which further constrains the temperature of the electrum emplacement. The salinity of the two phase inclusions was also low, being on average 2.8 ± 2.2 eq. wt% NaCl (1σ). This low salinity fluid was further supported by Raman spectroscopy/spectrometry, as the shape of the liquid curve was indicative of a low salinity fluid. Raman spectroscopy/spectrometry identified methane and nitrogen as volatiles, which is to be expected in a shallow environment, though no signature of CO_2 was found. The lack of CO_2 is not normal for orogenic systems, which often have moderate amounts of CO_2 as a vapour phase. "Hot cathode" cathodoluminescence showed that the quartz had undergone low grade metamorphism. SIMS analysis based on cathodoluminescence mapping of a quartz sample containing electrum found the Maisie quartz vein has a $\delta^{18}O_{V\text{-}SMOW}$ composition ranging from 12.3 – 18.8 ‰. Based off of the $\delta^{18}O$ quartz composition, the initial fluids sourcing the gold would have had to have a $\delta^{18}O$ composition ranging from 7 – 18.5‰. Seeing that the system was low pressure, and doesn't show any signs of high grade metamorphic minerals, the more likely value of the initial quartz-forming fluids would be ~7 ‰, falling in the range of formational fluids. These findings support this electrum occurrence being an epizonal-orogenic gold system. Further study is needed to confirm this type of classification.

References

Annels AE, Roberts DE (1989) Turbidite-hosted gold mineralization at the Dolaucothi gold mines, Dyfed, Wales, United Kingdom. Economic Geology; 84(5):1293-314

Bertrand R, Malo M, Lavoie D (2005) Thermal Maturation and Hydrocarbon Potential of Ordovician to Devonian Rocks in Northwestern New Brunswick. In2005 AAPG Annual Convention

Bodnar RJ, Vityk MO (1994) Interpretation of microthermometric data for H2O-NaCl fluid inclusions. Fluid inclusions in minerals: methods and applications: p. 117-30

Boggs Jr S, Young-Ihn K, Goles GG, Rusk BG, Krinsley D, Seyedolali A (2002) Is quartz cathodoluminescence color a reliable provenance tool? A quantitative examination: Journal of Sedimentary Research; 72, p 408‑415

Carroll JI (2000) Geology and geophysics of the east half of the Kedgwick map area (NTS 21 O/11 east), northern New Brunswick. In: B.M.W. Carroll (ed.), Current Research 1999. New Brunswick Department of Natural Resources and Energy, Minerals and Energy Division, Mineral Resources Report 2000-4, pp. 1-16

Carroll, JI (2003a) Geology of the Kedgwick, Gounamitz River, States Brook and Menneval map areas (NTS 21 O/11, 21 O/12, 21 O/13, and 21 O/14), Restigouche County, New Brunswick., pp. 23-57. In: B.M.W. Carroll (ed.), Current Research 2002. New Brunswick Department of Natural Resources; Minerals, Policy and Planning Division, Mineral Resources Report 2003-4

Carroll JI (2003b) Geology of the Menneval area (NTS 21 O/14), Restigouche County, New Brunswick New Brunswick Department of Energy and Mines, Map plate MP 2003-26, 1:50 000 scale

Carroll JI (2005) Geology of the Kedgwick (NTS 21 O/11), Gounamitz River (NTS 21 O/12). States Brook (NTS 21 O/13), and Menneval (NTS 21 O/14) map areas, northwestern New Brunswick. New Brunswick Department of Natural Resources, Minerals, Policy and Planning Division; Plate 2005-57

Castelli D, Rolfo F, Groppo C, Compagnoni R (2007) Impure marbles from the UHP Brossasco-Isasca Unit (Dora-Maira Massif, western Alps): evidence for Alpine equilibration in the diamond stability field and evaluation of the X (CO2) fluid evolution. Journal of Metamorphic Geology; 25(6):587-603

Castle Resources Inc. (2010) Castle Resources Completes 4,000 Metre Drill Program at Its Elmtree Gold Project, New Brunswick. http://www.marketwired.com/press-

release/castle-resources-completes-4000-metre-drill-program-its-elmtree-gold-project-new-brunswick-tsx-venture-cri-1371969.htm

Chi G, Dubé B, Williamson K, Williams-Jones AE (2006) Formation of the Campbell-Red Lake gold deposit by H2O-poor, CO2-dominated fluids. Mineralium Deposita;40(6-7):726-41

Corbett G (20002) Epithermal gold for explorationists. Abstract for AIG Journal, Paper

Davies JL (1977) Geological Map of Northern New Brunswick. Department of Natural Resources

Driesner T (2007) The system H 2 O–NaCl. Part II: Correlations for molar volume, enthalpy, and isobaric heat capacity from 0 to 1000° C, 1 to 5000bar, and 0 to 1 X NaCl. Geochimica et Cosmochimica Acta; 71(20):4902-19

Driesner T, Heinrich CA (2007) The system H 2 O–NaCl. Part I: Correlation formulae for phase relations in temperature–pressure–composition space from 0 to 1000° C, 0 to 5000bar, and 0 to 1 X NaCl. Geochimica et Cosmochimica Acta; 71(20):4880-901

Eremin RA, Voroshin SV, Sidorov VA, Shakhtyrov VG, Pristavko VA, Gashtold VV (1994) Geology and genesis of the Natalka gold deposit, Northeast Russia. International Geology Review; 36(12):1113-38

Faure G, Mensing TM (2005) Isotopes: principles and applications. John Wiley & Sons Inc

Garnier V, Malo M, Dubé B, Chagnon A, Beaudoin G (2007) Carlin-type gold mineralization at Saint-André-de-Ristigouche, Gaspé Peninsula (Québec), Canadian Appalachians. Mineralium Deposita; 42(6):639-62

Goldfarb RJ, Groves DI, Gardoll S (2001) Orogenic gold and geologic time: a global synthesis. Ore geology reviews; 18(1):1-75

Goldfarb RJ, Baker T, Dube B, Groves DI, Hart CJ, Gosselin P (2005) Distribution, character, and genesis of gold deposits in metamorphic terranes. Economic Geology 100th anniversary volume; 40

Goodfellow WD, McCutcheon SR, Peter JM (2003) Massive sulfide deposits of the Bathurst Mining Camp, New Brunswick and Northern Maine: Introduction and summary of findings. Economic Geology Monograph; 11:1-6

Groves DI, Goldfarb RJ, Gebre-Mariam M, Hagemann SG, Robert F (1998) Orogenic gold deposits: a proposed classification in the context of their crustal distribution and relationship to other gold deposit types. Ore geology reviews; 13(1):7-27

Hallbauer DK (1986) The mineralogy and geochemistry of Witwatersrand pyrite, gold, uranium, and carbonaceous matter. In Mineral deposits of Southern Africa V 1-2

Harris DC (1986) Mineralogic report on samples from the Elmtree Deposit, Energy Mines, and Resources, Canada, Unpublished Company Report

Kerrich R, Wyman D (1990) Geodynamic setting of mesothermal gold deposits: An association with accretionary tectonic regimes. Geology; 18(9):882-5

Lentz DR, Goodfellow WD, Moore CE (1995) The geological significance of the alkalic gabbro in the immediate hanging wall to the Brunswick No. 12 massive sulphide deposit. Bathurst, New Brunswick: Geological Survey of Canada Paper, 233-43

Lentz DR, Thorne KG, Yang XM (2002) Preliminary analysis of the controls on the various episodes of gold mineralization at the Lake George antimony deposit, New Brunswick. Current research: 02-1

Malo M, Béland J (1989) Acadian strike-slip tectonics in the Gaspé region, Québec Appalachians. Canadian Journal of Earth Sciences; 26(9):1764-77

Malo M, Bourque PA (1993) Timing of the deformation events from Late Ordovician to Mid-Devonian in the Gaspé Peninsula. Geological Society of America Special Papers; 275:101-22

Malo M, Moritz R, Dube B, Chagnon A, Roy F, Pelchat C (2000) Base metal skarns and Au occurrences in the southern Gaspé Appalachians: distal products of a faulted and displaced magmatic-hydrothermal system along the Grand Pabos-Restigouche fault system. Economic Geology; 95(6):1297-318

Mao J, Konopelko D, Seltmann R, Lehmann B, Chen W, Wang Y, Eklund O, Usubaliev T (2004) Postcollisional age of the Kumtor Gold Deposit and timing of Hercynian events in the Tien Shan, Kyrgyzstan. Economic Geology; 99:1771 – 1780

McClenaghan SH, Goodfellow WD, Lentz D (2003) Gold in massive sulfide deposits. Bathurst Mining Camp: Distribution and genesis: Economic Geology, Monograph; 11:303-26

McFarlane CR, Mavrogenes J, Lentz D, King K, Allibone A, Holcombe R (2011) Geology and intrusion-related affinity of the Morila Gold Mine, southeast Mali. Economic Geology; 106(5):727-50

Meinhold G (2010) Rutile and its applications in earth sciences. Earth-Science Reviews; 102(1):1-28

Mernagh TP, Wilde AR (1989) The use of the laser Raman microprobe for the determination of salinity in fluid inclusions. Geochimica et Cosmochimica Acta; 53(4):765-71

Morrissy C (1991) Gold assessment at Lake George mine, York County, New Brunswick. New Brunswick Department of Natural Resources and Energy, Mineral Resources, Open File Report 91-1, p 22Parkhill, MA (2005) Till Geochemistry of the Kedgwick, Gounamitz River, States Brook, and Menneval Map Areas (NTS 21 O/11, 12, 13, and 14), Madawaska, Restigouche, and Victoria Counties, Northwestern New Brunswick. Open Fill, New Brunswick Natural Resources, Minerals, Policy and Planning; OF2005-4

Paton C, Hellstrom J, Paul B, Woodhead J, Hergt J (2011) Iolite: Freeware for the visualisation and processing of mass spectrometric data. Journal of Analytical Atomic Spectrometry; 26(12):2508-18

Ramsay WR, Bierlein FP, Arne DC, VandenBerg AH (1998) Turbidite-hosted gold deposits of Central Victoria, Australia: their regional setting, mineralising styles, and some genetic constraints. Ore Geology Reviews;13(1):131-51

Riva J, Malo M (1988) Age and correlation of the Honorat Group, southern Gaspé Peninsula. Canadian Journal of Earth Sciences; 25(10):1618-28

Ruitenberg AA, McCutcheon SR, Watters SE, Mc-Leod MJ, Burton DM, Hoy D (1989) Field guide to gold occurrences in New Brunswick: New Brunswick Department of Natural Resources and Energy. Minerals and Energy Division, Field Guidebook; 1:63Ryan RJ, Smith PK (1998) A review of the mesothermal gold deposits of the Meguma Group, Nova Scotia, Canada. Ore Geology Reviews; 13(1):153-83

Rye DM, Rye RO (1974) Homestake gold mine, South Dakota; I, Stable isotope studies. Economic Geology; 69(3):293-317

Sharp ZD, Kirschner DL (1994) Quartz-calcite oxygen isotope thermometry: a calibration based on natural isotopic variations. Geochimica et Cosmochimica Acta, v. 58, p.4491-4501.

Schwarz S, Lentz DR, Walker JA (2007) Gold deposits in the Elmtree Inlier, northeastern New Brunswick. *In* Abstracts 2007: Exploration and Mining New Brunswick.

Edited by Merlini SAA. New Brunswick Department of Natural Resources, Minerals Policy and Planning Division, Information Circular 1, p. 41–42

SLAM Press Release (2012) SLAM Trenches New Gold-Bearing Vein, Source Of Maisie Zone Boulders Found In 155 m Long Quartz Vein. http://www.marketwired.com/press-release/slam-trenches-new-gold-bearing-vein-tsx-venture-sxl-1696477.htm

Stirling JAR (1987) Mineralogy of selected gold deposits in New Brunswick. New Brunswick Research and Productivity Council, p 25

Thomas JB, Watson EB, Spear FS, Shemella PT, Nayak SK, Lanzirotti A (2010) TitaniQ under pressure: the effect of pressure and temperature on the solubility of Ti in quartz. Contributions to Mineralogy and Petrology; 160(5):743-59

Thorne KG (2011) Gold. New Brunswick Department of Natural Resources; Lands, Minerals and Petroleum Division, Mineral Commodity Profile No. 8, p 8

Tomkins HS, Powell R, Ellis DJ (2007) The pressure dependence of the zirconium-in-rutile thermometer. Journal of Metamorphic Geology; 25(6):703-13

Watters SE (1993) Structure and alteration related to Hercynian gold deposition. Cape Spencer, New Brunswick, Canada [Ph. D. thesis]: London, Ontario, The University of Western Ontario

Wilde AR, Layer P, Mernagh T, Foster J (2001) The giant Muruntau gold deposit: geologic, geochronologic, and fluid inclusion constraints on ore genesis. Economic Geology; 96(3):633-44

Wilson RA (2003) Geology of the Upsalquitch Siding area (NTS 21 O/15d). Restigouche County, New Brunswick. New Brunswick Department of Naatural Resources, Minerals, Policy and Planning Division; Plate 2003-10

Wilson RA, Burden ET, Bertrand R, Asselin E, McCracken AD (2004) Stratigraphy and tectono-sedimentary evolution of the Late Ordovician to Middle Devonian Gaspé Belt in northern New Brunswick: evidence from the Restigouche area. Canadian Journal of Earth Sciences; 41(5):527-51